FOILING SuMoth CHALLENGE

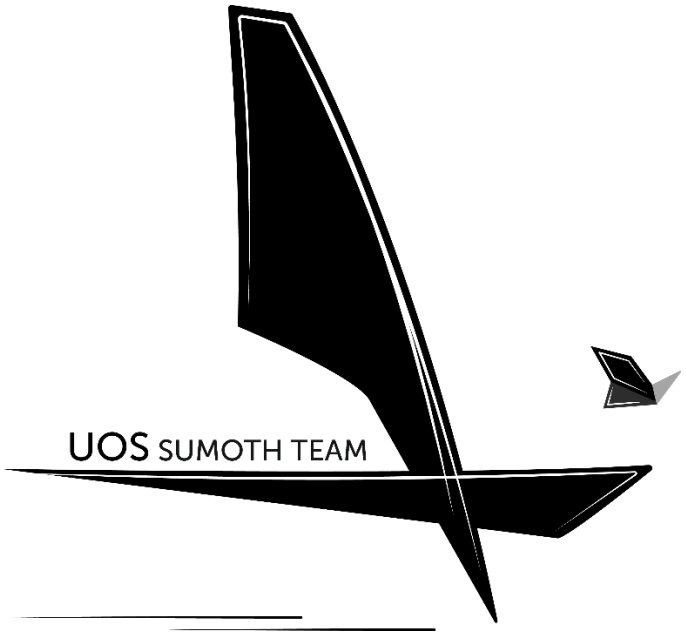

University of Southampton

Foiling SuMoth Challenge Stage 1 - 2024

DESIGN, MANUFACTURING & SUSTAINABILITY

sponsored by

11TH HOUR RACING

MARINESHIFT360

PERSICO

REPORT GUIDELINES

Bcomp®

TEAM NAME | UNIVERSITY NAME, CITY, COUNTRY | email@university.edu

INTRODUCTION

For this year's entry into the SuMoth Challenge, the team has built upon the legacy left by the 2022 group to explore the performance and sustainability of one of the most critical components on board. This was done in keeping with the team philosophy of continuously maintaining and improving the current platform, by the addition of more components fully manufactured in house. This year the chosen component was the main hydrofoil horizontal, which was thoroughly designed and optimised for hydrodynamic and structural performance and manufactured using alternative and expired materials and bio-based composite moulding techniques to reduce its overall environmental footprint.

Furthermore, to improve the team's understanding of the platform and create a framework for future development, a sensor suite was installed on board to track the boat's sailing performance and aid in further design. The set of electronics was also further developed into an easily adjustable ultrasonic ride height control system, which has the potential of improving the sailing performance by overcoming the wand's shortcomings.

The team was comprised of 6 Ship Science students of international backgrounds, representing Brazil, Uruguay, France, Ireland, Wales and England. The team's technical roles were divided based on interest and previous experience, with two student focusing on the electronics and sensors while the other 4 were dedicated to the hydrofoil design and manufacture, as well as the sustainability evaluation.

To accomplish a design that balanced performance and sustainability, the MarineShift360 software was employed over all design iterations as a means to judge the effectiveness of design choices in tackling the environmental impact of the foil and help guide the team to achieve the goals set out. The final hydrofoil was manufactured using a sustainably grown timber mould and includes a flax fibre core laminate and flap, completed with expired carbon fibre pre-preg outer skins, and showed a 10% higher stiffness that the baseline, industry-produced foil used in the previous setup and a near 90% reduction in CO2eq emissions associated with its manufacture.

ACKNOWLEDGMENTS

1. The University of Southampton, for the provision of funding, use of tools and facilities.
2. Maguire Boats, for the provision of materials and expert advice.
3. Professor Stephen Boyd and Dr James Blake, for the supervision of the project and expert advice and assistance.
4. Previous benefactors and sponsors, for helping the previous GDP group build the boat.
5. Damian McLellan and Joe Wright, for their technical help and support.
6. Christopher Lum, for his expertise on control system and engaging lecturing.
7. Ellen Driver, for allowing the use of her rigid hull inflatable boat as a safety boat when testing.

LIST OF TABLES

LIST OF FIGURES

1. ENGINEERING AND DESIGN

1.1. State of the art

To further develop the previous campaign, we have spent the last few months working on improving key aspects of the vessel we hope will work to revolutionize the industry and build a solid platform for future teams to expand on:

We have created an electronic data acquisition and telemetry system to track and log the boat's sailing performance and send out live data, which can be streamed on the internet during a race, allowing the team and anyone watching to follow the action live. Furthermore, the boat sailing data was applied to a newly developed electronic ride height control system based on an ultrasonic distance sensor fused with an IMU and GPS. The controller functions at high measurement frequency and allows the boat to filter off waves operate consistently in different weather states. The post processing of the data collected is expected to give great insight into the boat's performance and allow the team to understand the areas of the project that require improvements and aid in future design.

We have designed a hydrofoil section from scratch utilizing a novel Machine learning approach employing a powerful GAN based algorithm to optimize for a high efficiency, high lift foil that is designed around our expected operating parameters. This foil design has been identified for use based on the operational window provided by the telemetry and structural adaptations to enable us to incorporate flax fibres and bio-resin to reduce our overall carbon content to 58% for the main hydrofoil. The design has been optimised to maintain similar take-off characteristics as our original section while maintaining greater lift to drag coefficients over most of our operational window.

1.2. Hydrofoil Redesign

The Design of the vessels Hydrofoils is an extremely complex, iterative process which constitutes a significant portion of the vessel's overall performance characteristics. For this design a thorough understanding of the deign aspects in play is crucial in isolating the problem in hand and adapting our design to reach optimum performance while keeping things such as structural, and manufacturability requirements under control. Time also must be taken to ensure the reaction of the foil over the entire operating region remains correct and does not significantly impact the vessels handling characteristics.

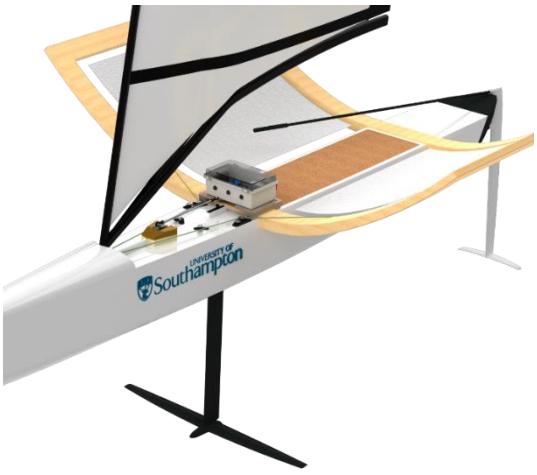

For this entry of the SuMoth we have focused on manufacturing the main hydrofoil only, as, due to time constraints, we were unable to produce a rudder foil and rear vertical in our available timeframe. During the design phase of this project, we were continually focused on ensuring the sustainability of our final project, utilizing more sustainable materials such as flax based on research from the previous project, to reduce our carbon content as well as looking at key energy and emission contributors such as the mounds of the foil.

1.2.1. Performance Optimization vs. Sustainability

Advancements in hydrofoil design have come along leaps and bounds, from empirical scaled models to CFD and AI-Driven Optimization. CFD, however, is very computationally intensive and thus a compromise with an alternative approach must be made in the name of sustainability to minimize our computational load and subsequent energy consumption. This would reduce the impact on the environment during design. The problem with conventional CFD approaches lies in the generally lose-lose situation. Performance can be analysed thoroughly, giving good performance but bad environmental impact, or traded in the name of sustainability. Therefore, a compromise may be made using CFD alternatives and optimization methods.

1.2.2. Our Optimization Algorithm

A machine learning algorithm was chosen for our optimisation due to its adaptability both for this use case, along with commercial applications relating to foil design and hull forms. Using the machine learning approach was favoured over a genetic algorithm or manual regression as the speed and capability to explore the design space, without coding based constrains over defining the available solutions, is beneficial.

Although the machine approach is not necessarily the most energy efficient due to initial computational setup costs, it allows a quick generation and analysis of possible performant foils. Additionally, the design space can be probed to arrive at a Pareto front of the top 20 foil designs found based on lift-to-drag ratios (Cl/CD) for the 2D optimal foil design. This was based on the specific inputs of Reynolds number, Mach number and optimal AoA in a short period of just over three hours.

After investigations into reinforcement learning, such as convolutional graphical neural networks, the lack of publicly available data prevented the generation of the required data amount to train a reinforcement-based model. This was deemed unsustainable and beyond the scope of our project, as this would better fit a dataset built-up gradually overtime as a byproduct of experimental testing. An alternative machine learning approach found to be applicable to this use case was a GAN which works via two pathways. As shown in Figure 3, the generator section focuses on learning patterns from the training data set, generating new foils based on this pattern, while a discriminator works on identifying foils created by the generator by comparing the foils to a sample batch of the real foil data. This allows for a significant spread of foil designs over the possible design space to be generated by the GAN and analysed using XFOIL.

As an example of the efficiency gain by using XFOIL instead of fully fledged CFD software, the machine learning model can produce 19000 foils in 194mins at 125 watts based on a Quadro P4000 and Zeon E5-2620 V3. For comparison, Ansys CFD could only analyse 16 foils in 194mins at 190 watts using the same setup. Generally, the GAN produces 1000 usable foils per operation cycle, giving 95 times increase in performance in terms of foils per-watt (FpW) (2.47 vs 0.026 FpW) for 2D foil sections. Note for CFD this only accounts for the analysis not generation of the foil design.

1.2.3. Performance Validation

To ensure our method is viable, we have constructed and compared the outputs of out model to Singular Value Decomposition (SVD) and Free Form Deformation (FFD) models, as shown in Figure 1. These algorithms specialise in efficiency and flexibility respectively and provide a good basis for comparison between both the systems and the GAN itself as its parameters are tuned. Additionally, the new foil was compared to previous existing moth foils. As can be seen in Figure 1 we were unable to constrain the SVD model and thus many of the most performant foils were unmanufacturable. The foils from FFD and GAN models were more manufacturable.

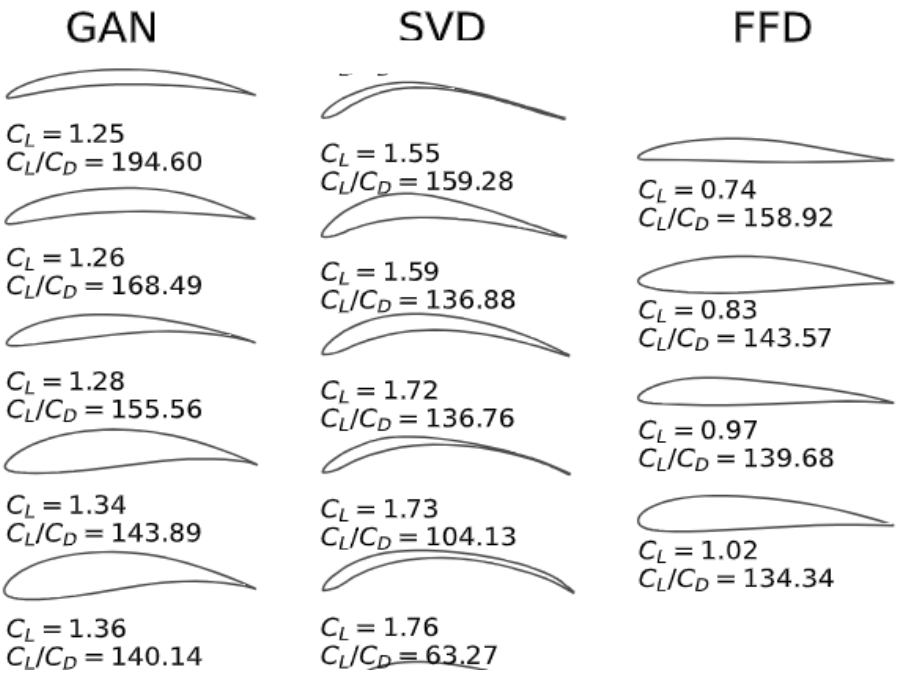

Figure 1 - Comparison of GAN, SVD and FFD algorithm results.

1.2.4. GAN Training Loop

The GAN algorithm developed is an adaptable multi-element approach using a Bezier foil parameterisation with an additional Detrimental Point Process (DPP) kernel incorporated into the training to help the GAN produce more foils on the Pareto front. Additionally, an optional Bayesian optimisation is conducted on the trained model to further improve the performance of our design after an initial production of a data set. The Bayesian optimisation generates a probability model of the GAN using hyperparameters to tune the model. This optimisation was iterated through 150 times per data set, with 10 data sets being selected from the initially produced set of foils in the first design loop of Figure 6. As shown in Figure 2, at 124 operations there was a peak in performance with the hypervolume indicator (a measure of the quality of the tuning) reaches its maximum value at this point.

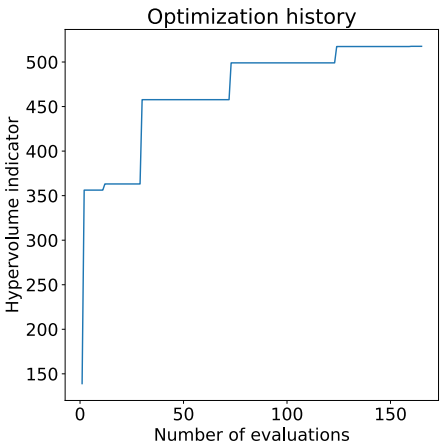

Figure 2 - Hypervolume indicator.

The tuning was assessed and 100 foils from each of the 10 sets were produced using the trained Generator. The inputs to the model are noise (matrices Z1 to Zn) and optimal conditions parameters (values W1 to Wn) such as pitch angle, Mach number and Reynolds number. 2D foil sections are collected from the UIUC aerofoil database, pre-processed and converted to a Bezier parameterised foil. Following the flow chart in Figure 3, UIUC data is split with most of the data going to the generator and a randomised sample set sent to the discriminator. Generated designs are then sent to both the discriminator to filter out invalid designs against the selection of database test foils and the optional DPP kernel. The GAN was set up to maximise lift-to-drag ratio for the foils while also optimising for lift.

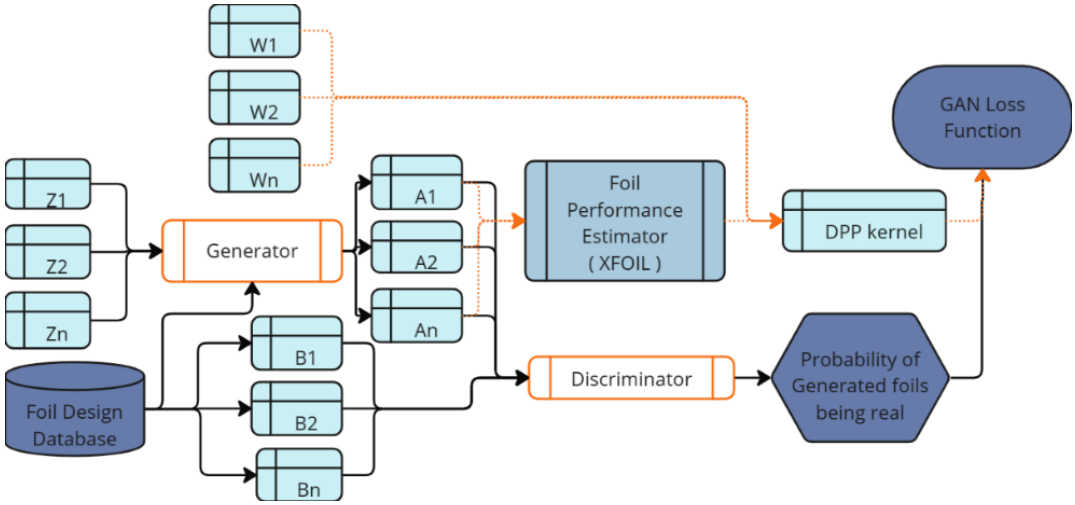

Figure 3 - GAN training loop.

1.2.5. Determinantal Point Process (DPP) Kernel

The DPP kernel is used to prevent mode collapse where GAN fails to capture the diversity of the data. This is done by modifying the GAN loss function which gets fused into the trained GAN. The kernel prevents mode collapse by modelling negative correlations between subsets of foil data and applies corrections In line with the noise while trying to understand the effects of change on the foil shape. To do this, our performance estimator calculates the lift and drag of the foils before being fused with the DPP kernel in addition to the foil parameters. This process subsequently leads to designs that more efficiently explore the design space as shown in Figure 4.

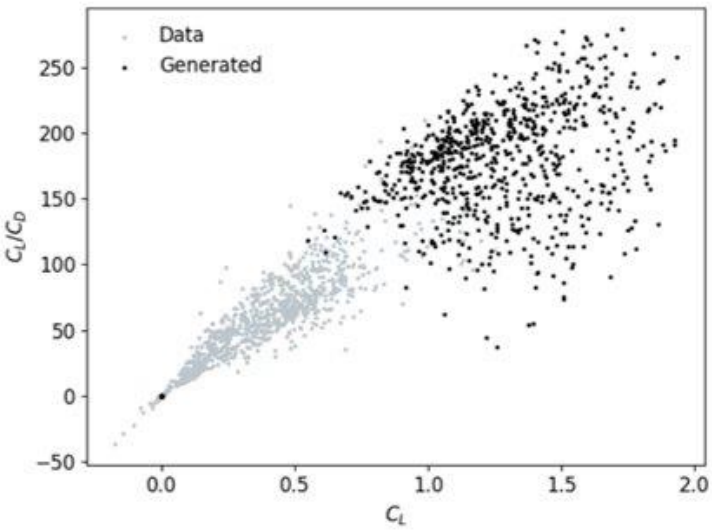

Figure 4 – GAN Design Space Exploration.

1.2.6. Parameterisation.

To reduce the number of inputs into the system the foil was parameterised using a 31 degree-of-freedom Bezier curve to model the foil, an example of which can be seen in Figure 5. This method was chosen over parameterisation methods, such as PARSEC, as Bezier is limited to smooth curves and is not overly constrained, therefore eliminating resolution issues. By reducing the inputs, changes in the GAN parameters have a larger, enabling it to determine the consequences of parameter modification. Additionally, with less control points, this parameterisation allows us to operate the design processor faster and be more efficient with our resources.

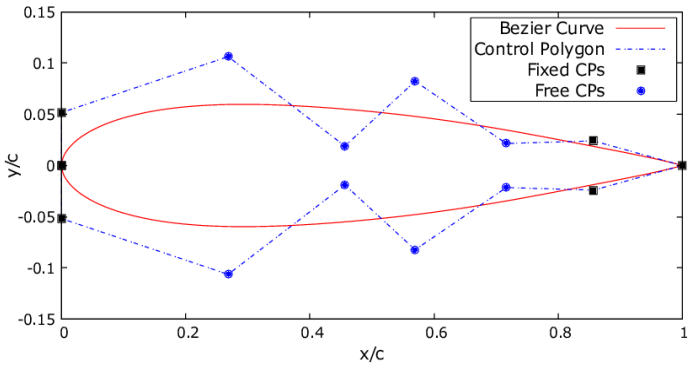

Figure 5 - Bezier parameterisation example.

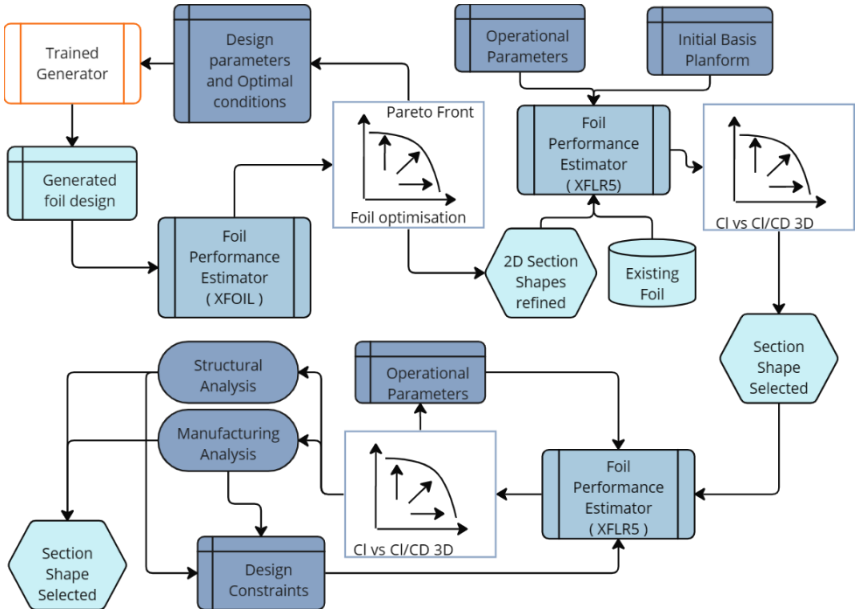

Figure 6 - Foil design loop.

1.2.7. Using the Trained GAN Foil Generator

The GAN, once trained on the UIUC dataset with its optimisation parameters and conditions, we are presented with a range of optimal solutions along the Pareto front comparing lift-to-drag ratios with total lift. The selection of foils from Figure 1 would subsequently be filtered based on manufacturability of foil geometry, before a final comparison of the sections was completed. To check the refined foil sections, the original H105 foil was modelled in XFLR5 in Figure 6 without a fuselage and modified with the new sections to compare the performance as part of an established planform.

The foil was modelled without a central fuselage to ensure a fair comparison took place as some foil shapes would not be able to operate with the existing fuselage. Additionally, there was a risk that the fuselage trips turbulence in the flow. Throughout the design process care has been taken to minimise turbulent flow as XFLR5 is limited in its response and calculations of viscous effects, relying on modification factors and empirical data to accommodate the viscosity of the fluid.

The XFLR5 results allowed the team to compare important characteristics such as lift-to-drag curves, induced and parasitic drag along with pitch stability. The foil was assessed at take-off speed and at an estimated top speed allowing us to compare lift and deduce the range of foil response during the acceleration phase. These results were then used to select the 2D section. Once the section was selected, variations in span, chord, taper ratio, aspect ratio and area were completed and analysed in conjunction with the structural response and manufacturing to influence the design constrains before a final foil was selected. The structural analysis was conducted on multiple foils including the final form to ensure compliance within structural limits.

1.2.8. Selecting the 2D Foil

To select the correct foil for our purpose, a range of 30 hydrofoils collected over multiple runs were selected from the GAN generation data. Foils were also compared from the SVD and FFD models, however the manufacturing and or performance generally made these non-competitive. The new sections were input into XFLR5 and manually tested using the existing old foil parameters as a base platform for calculating lift and drag, along with utilising the existing operational parameters of the foil.

The H105 was also left in our processing as a baseline foil for comparison. The selected sections were analysed at 4ms-1 and 11.4ms-1 at angles ranging ±8 degrees. Foils were compared against drag components, lift-to-drag ratio and pitch stability. Once the analysis was performed, the selected foils were compared against each other and the existing foil, determining a successful candidate named AF153. As shown in Figure 7, the foil has been plotted against the current H105 foil alongside another initial competitor that neglected due to manufacturing constraints.

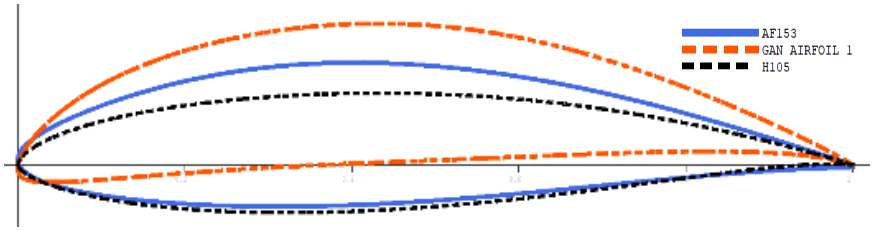

Figure 7 – Foil section comparison

The final foil is similar to the H105 with a stouter nose and a 20% thicker midsection, tapering off earlier to a flatter lower aft section. It should be noted that high performance foil sections that are not publicly available were omitted from the training data such as the H105. The flatter rounder nose will increase the pressure gradient slightly but is necessary to incorporate the thicker midbody. The midbody thickness will work to increase the pressure differential between the upper and lower surfaces. The tail flattening modifies the flow off the foil, aligning the flow helping extend the pressure differential aft. This foil section has a Cl=136 & Cl/Cd 145.2.

1.2.9 XFLR5 and XFOIL

XFLR5 and XFOIL are free opensource CFD software which work by using panel methods and boundary layer theory with XFLR5 expanding on XFOIL by utilising a vortex lattice method for 3D capabilities. While XFOIL can be automatically called via scripts, XFLR5 is restricted to manual operation. CFD software based on RANS or LES are well established within research and industry akin to XFOIL and XFLR5 however the computation reduction by going with these two software packages is nearly 100 times less demanding along with proven and reliable baseline performance.

1.2.10 Finalising the 3D Foil

During the finalisation process, checks were carried out to ensure ventilation was unlikely to occur, provided the foil, maintained flight below the 350mm depth marker on the vertical. This was checked by looking at the pressure gradient and magnitude to ensure atmospheric air would not travel down the vertical during operation. The final 3D AF153 foil section using the existing H105 planform underwent significant analysis in search of optimal geometry. Hydrofoil parameters such as span, area, root chord, AR and taper ratio were analysed for their effects.

Overall, the shape was altered up to ±30% of the basis foil parameters in approximately 5% steps. Where parameter alterations were clearly not producing more performant foils, parameter variation was halted for that region. Twist, sweep and dihedral angle were limited due to foil hinge geometry along with difficulty Analysing the real-world performance of these foils using XFLR5 due to its calculation constraints.

In total, eight varied foil designs were produced. High aspect ratios tended to have greater results due to the less induced drag but increased structural complexity. The chord variations provided similar resultant factors; it was found that delaying the taper along the span provided better results. As the AF153 foil section produced greater lift, a shorter span was selected to ensure the foil was strong enough while producing an overall greater lift force. An initial high aspect foil and H105-like hydrofoil were produced and provided to the structural team. Once processed, the substitution of carbon with alternate materials had restricted us to producing foils with a lower aspect ratio only, even with the increased section thickness. These loading and safety parameters could in future be more refined with an increase in data recorded from telemetry and foil structural testing.

Using telemetry data analysis from the control system, several foil structures were calculated before a final foil design was produced. This data was subsequently plotted and analysed to see the response of the final foil. A comparison of three of the best performing foil designs is provided in Table 1 with performance displayed in Figure 8.

The high aspect AF153 was included in the table to show the possible performance gains, however it was deemed unmanufacturable due to structural limitations. The AF153 #5 produced has on average 56% higher lift coefficient while having a 30% greater lift-to-drag coefficient at 4ms-1 at 0° AOA as seen in Figure 8. Due to the smaller AR and area, this translated to a 9.8% increase in lift (175N to 192N) compared to a 9% increase in drag (6.8N to 7.4N). In addition to this lift increase, our foil maintains a higher lift-to-drag ratio between -5 and 2.6 or 0.5° for low and high speed, respectively. Therefore, across the Moth's foil operating range there is an efficiency gain with top end efficiency losses negated by Moth tendencies to sail nose down to reduce lift at higher speeds.

Analysing take-off speed, the foil and flap were angled to +5° and -5° respectively to generate maximum lift. With the main foil calculated to take 70% of the lift and a total weight of 149.35kg, a lift force of 1025.6N was calculated. Analysing the foil, it sits within the 10% speed difference design requirement. To achieve this, an additional 0.3 ms-1 from 4.86 to 5.16 ms-1, this does come however with a 5% reduction in drag. This drag may not be realised due to non-foiling hull drag but this too could be overcome by pumping the Moth, which utilises the brief reduction in hull drag to accelerate the vessel onto its foils. This would be within the margin of error of XFLR5. Our 3D foil was calculated to have CL= 0.365 at 0° with CL/CD= 25.58 and 75.58 for 4 and 11.4m/s respectively.

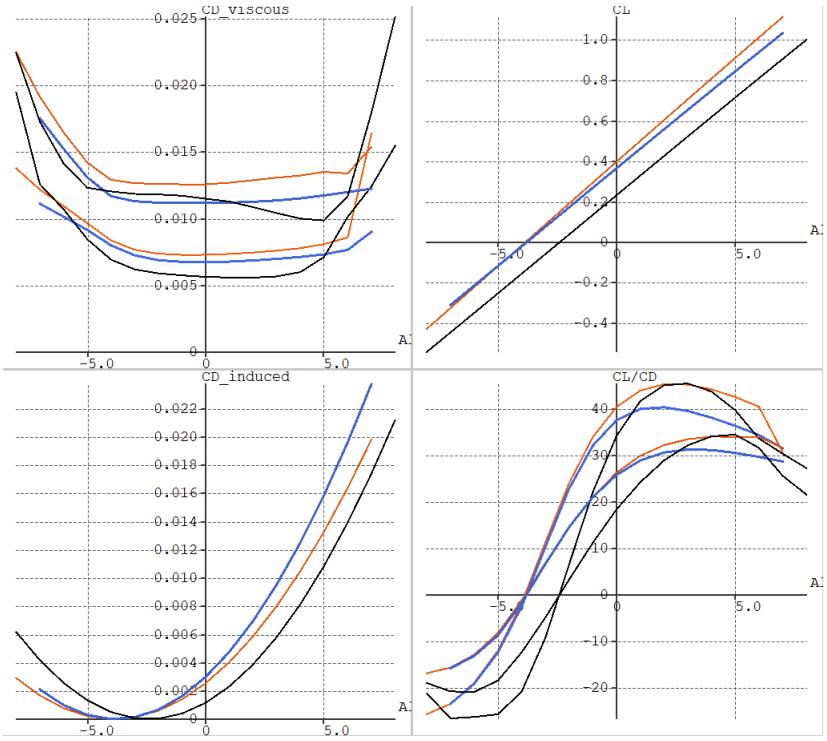

Figure 8 – Foil Comparison of foils H105-Black, AF153-Blue, and high aspect AF153-Orange.

Table 1 – Foil Parameters

Parameter	*AF135 #5*	*H105*	*High aspect AF135 #8*
Span	1	1.12	1.15
Area	0.07	0.084	0.069
Root chord	0.087	0.1	0.08
MAC	0.73	0.082	0.65
Aspect Ratio	14.283	14.938	19.173
Taper Ratio	0.46	0.26	0.26

1.2.11 Final Steps

After finalising the foil shape, the foil was provided to manufacturing and structures to analyse. Once checked, the foil fuselage and flap designs were added to the overall design. The manufacturing team designed the foil flap mechanism and were able to capture the fuselage off the original H105 foil. These components were applied to our finalised design. Overall, a parametric CAD model was used to iterate the foil design, assisting structural testing and mould making. Below we have a Figure 9, showing the final 3D Render of the foil with the fuselage attached before production.

Figure 9 - 3D Render of Final AF153 Foil.

1.3. Structural Analysis

Structural analysis was an integral part of the design process and a constant consideration in the design loop alongside performance and manufacture. The technology behind high performance hydrofoils, such as the main foil that is being manufactured for the *SuMoth Challenge*, have advanced considerably with the increasing availability of composite materials which offer high strength and stiffness to weight ratios [1]. For applications such as hydrofoils, maintaining a low weight is paramount when considering the structural design. As a result, top of the range Moth foils available on the market are manufactured using 100% carbon fibre reinforced polymers (CFRP).

When considering the material specification for the hydrofoil, the key considerations were maintaining a high-performance design through minimising the weight, whilst also improving the sustainability of the foil through the use of alternative composites. The *SuMoth Challenge* rules prohibited the total mass of the epoxy reinforced carbon fibre included in the foil to exceed 60% of the total mass. This provided a significant structural challenge, since removing carbon fibre from the lay-up to be replaced with less stiff, heavier materials has a negative impact on the performance of the hydrofoil. Firstly, a heavier foil would increase the amount of lift required for the boat to fly. Additionally, a less stiff foil will experience larger tip deflections and twist. Implications of this include reduced hydrodynamic performance through increased angles of attack towards the tip, potentially leading to flow separation. Furthermore, excess tip deflections and twist can reduce the performance of the hinge connection between the main foil section and the flap, reducing the responsiveness of the flap to the control system.

1.3.1. Section Shape

The section shape was a key area of the design loop between performance and structural design. Since CFRP has by far the most optimal stiffness to weight ratio, the decision was made to use the 60% weight restriction to build a 3mm skin around the foil, thus ensuring that the strongest materials are positioned furthest from the neutral axis and maximising the stiffness.

Since modern hydrofoils are built with 100% carbon fibre, it was necessary to increase the section thickness compared to a standard Moth foil to further move the carbon skin away from the neutral axis. Although this causes a reduction in efficiency, it allows for the stiffness of the foil to match an industry designed foil whilst reducing the carbon content of the laminate. Equally, any excessive bending or twist would negate any performance gains that would be provided by a thinner foil section.

1.3.2. Laminate Specification

Selecting a suitable laminate specification was vital from a structural perspective. Changes in the layer orientation significantly impacted the mesostructure of the laminate, thus influencing the properties of the foil [2]. With most of the foil stiffness being provided by the carbon skins, ensuring that the laminate orientation provided optimal properties for stiffness was a key consideration in both the structural and manufacturing design processes. Various layups were iterated, with considerations such as ease of manufacture, availability of materials and structural integrity being at the forefront.

Initially, a ply layup of [0/90, 0, 0, 0, ±45]s was considered, providing excellent stiffness when trialled in FEA. A symmetric layup was used in order to remove any likelihood of the material warping during the curing process. Providing enough unidirectional fibres along the span of the foil was the key driving factor for stiffness. Equally, bi-axial and woven plies provide stiffness against torsional forces, whilst also providing interply friction; a key factor in minimising the interply shear stress [3]. Manufacturing considerations provided changes to the layup, with the ±45° plies moved to the outer layers of the skin because they are more malleable and therefore provided a more compliant material to improve the finish of the foil, matching the surface of the mould better than other orientations.

The final laminate specification was determined to be [±45, 0, 0, 0/90, 0]s, providing the maximum number of unidirectional plies, whilst aligning with manufacturing guidelines by dispersing the unidirectional plies every two layers. The final lay-up provided the optimum balance between structural and manufacturing requirements, with enough variety in fibre orientation to provide interply friction and reducing the shear stress.

1.3.3. Foil Testing

The key goal of the FEA conducted on the hydrofoil was to understand the structural implications of design considerations proposed by the design team. Obtaining a perfectly accurate model was unrealistic due to the unpredictable nature of the manufacturing process, with uncertainties appearing in the following areas:

- The manufacturing process was very challenging and therefore the exact ply lay-up of the foil was impossible to replicate in a model. The complexity of the geometry resulted in variable ply overlaps and more or less layers than planned at certain points.

- Until very late on in the process it was uncertain what would constitute the core of the foil. Various solutions were considered, and even once flax fibres were decided upon, the resin content of the core was very difficult to control, thus providing uncertain material properties.

To mitigate the chance of uncertainties in the manufacturing process, compromising the overall structural integrity of the foil, the structural stiffness of the foil was assumed to entirely be provided by the carbon fibre skins. This is because carbon fibre provides a far greater stiffness-to-weight ratio than alternative available materials. Equally, the carbon skins are furthest from the foil neutral axis, thus providing the greatest stiffness. By considering the stiffness provided by the skins as the sole source, any additional stiffness provided by the core acts as a safety factor, therefore allowing unpredictable aspects of the wet lamination of the core, such as an excessive resin fraction would not prove to be critical. Although this provided a significant limitation in the structural analysis process, it allowed for the design to be optimised from a performance perspective without any uncertainty about the strength or stiffness of the foil.

1.3.4. Finite Element Analysis

The key consideration behind the development of a finite element model was the limited time available between receiving final design options and deciding on the final foil design. Therefore, work prior to the three final foil options involved producing an efficient and coherent model that would provide reliable results.

Mesh Convergence

To validate results and ensure that excess computational power was not expended, a grid independence study was carried out, concluding that increasing the number of nodes beyond 11000 provided very little benefit. Furthermore, the influence of refining the mesh around regions of interest such as the tip provided very little change in results. Therefore, a relatively coarse structured mesh was constructed for each foil, significantly accelerating the process and reducing the computational strain.

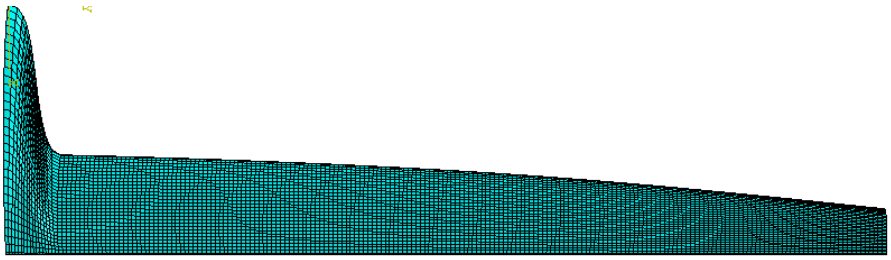

Figure 10 - Final mesh following grid independence study.

1.3.5. Final Foil Design Decisions

Towards the end of the foil design process with the final foil section already determined, it was necessary to consider the implications of various foil plan forms. The impact of changes such as aspect ratio, tapers and tip thickness have considerable influence on the performance of the foil. However, the foil with the best hydrodynamic performance may perform poorly if the wing experiences excessive deflections. Therefore, communication between the design, structural and manufacturing work packages was vital for this stage, with the final foil design best encompassing the requirements for each section.

The tip deflections for each foil design were determined by taking the spanwise bending moment distribution from XFLR5, assuming a worst case scenario. The negative of the second bending moment derivative therefore provided the load distribution on the foil, which was then divided by the average chord to provide the spanwise pressure distribution in Nmm^{-2}, therefore making it compatible with the Abaqus software. Equally, tip deflections were compared when subjected to a point load of 100N, however the pressure distribution provided the best information for how the foil will react under realistic loading conditions.

Foil AR17 had an aspect ratio of 17 and an aggressive taper towards the tip, therefore providing the most hydrodynamically efficient design. However, it experienced the largest tip deflection of 17.2mm. To produce the taper towards the tip, it was necessary to significantly reduce the number of plies in each skin, gradually reducing the thickness along the span, starting at 480mm from the root. As a result, the stiffness of the foil was significantly reduced towards the tip, the location of maximum deflection. When the reduced stiffness was combined with the increased difficulty of manufacture, the decision was made to consider lower aspect ratio foils and prioritise stiffer foils with an easier manufacturing process.

Consequently, foils AR15.6 and AR14 offered improvements in these areas whilst providing the same lift as AR17, albeit with an increased drag coefficient. AR15.6 and AR14 had aspect ratios of 15.6 and 14 respectively, with AR15.6 maintaining marginally more taper. The tip deflection of AR15.6 was 16mm, whilst AR14 had a tip deflection of 13.5mm. Similarly to AR17, the taper of foil AR15.6 meant that more plies needed to be removed towards the tip, reducing the stiffness of the foil and complicating the manufacturing procedure. The likelihood of errors in the manufacturing process, such as excess ply overlaps and inaccurate mould manufacture further encouraged the decision to select foil AR14, with no reduction of plies at the tip. Therefore, AR14 best encompassed the demands of the structural and manufacturing aspects of the foil design, whilst the drop-off in performance was not significant enough to warrant sacrificing these areas.

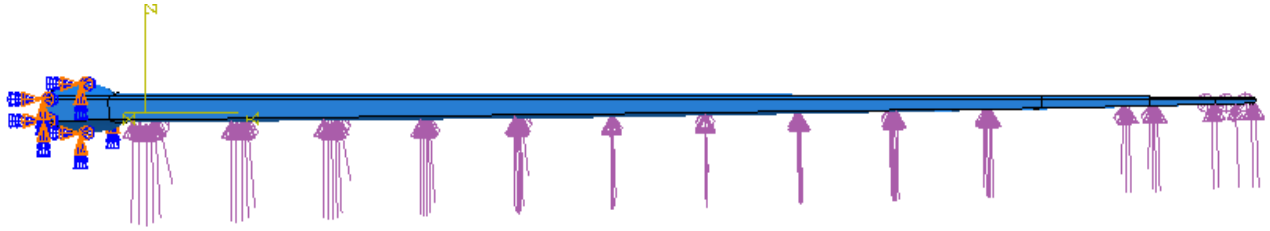

Figure 11 – Boundary conditions and pressure distributions for foil AR17.

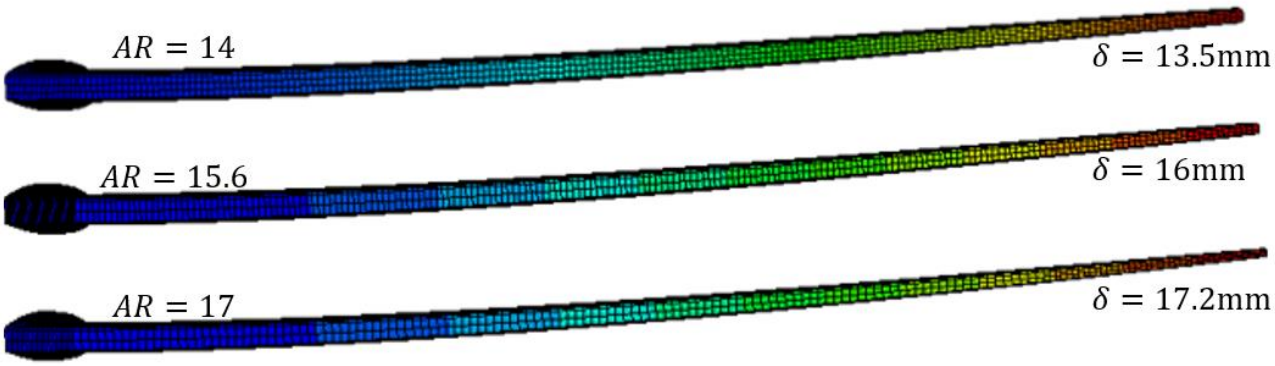

Figure 12 – Tip deflections under pressure loading for the three final foil designs. A deflection scale factor of 2 was applied to identify the differences between foils.

1.4. Data Acquisition

1.4.1. Background

As part of the design process of the new foil, the group needed to establish the baseline performance and overall boat attitude during sailing with the previous foil design. Due to the unpredictable and dynamic nature of the sailing conditions, laboratory testing would be insufficient to capture the boat behaviour. For this reason, the onboard data acquisition system shown in Figure 13 was developed to be mounted near the centre of gravity of the boat, designed to acquire real time sailing data while out on the water.

1.4.2. The Flight Computer

The data acquisition system employs a Raspberry Pi microprocessor (1) as the central computer to handle the real-time data feed from the sensors, as well as logging and sending that data to shore. The Pi was selected over a microcontroller as its more powerful computing capability enabled a streamlined development approach in CircuitPython and allowed the team to monitor the system remotely through a WI-FI hotspot, minimising the risk of water damage.

The flight computer sits inside a waterproof enclosure (2) along with the sensor hardware, radio and battery packs. Waterproof through wall connectors allow communication with external hardware.

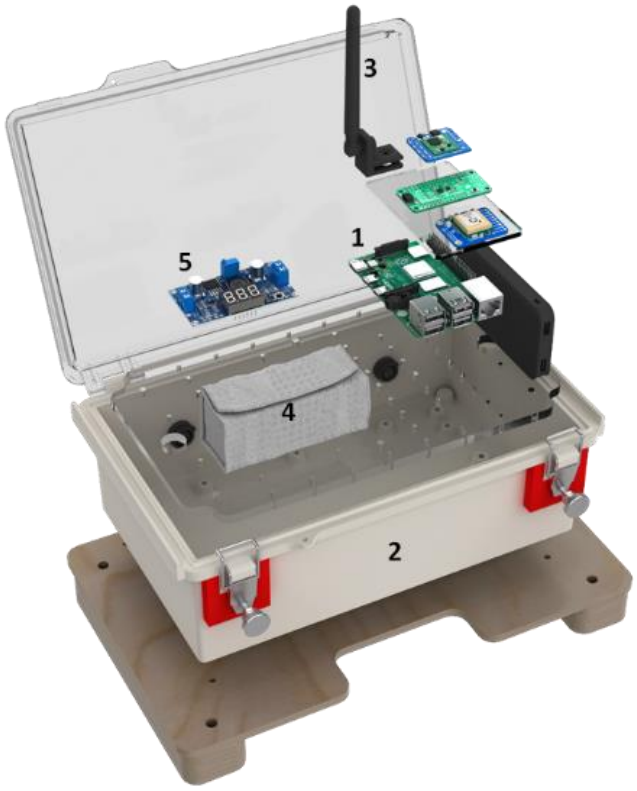

Figure 13 – Exploded view of electronics in data acquisition system.

1.4.3. Sensing & Fusion

To fully capture the boat's sailing behaviour a number of different sensors were selected. First and foremost, a 9-DoF Inertial Measurement Unit (IMU) was installed on board, which included 3-axis accelerometer, gyroscope and magnetometer. As we shall discuss later in this report, the combination of these three sensor's measurements allows us to estimate the absolute orientation of the vessel in space. In addition, an ultrasonic distance sensor was installed at the bow to measure the foiling ride height and a GNSS module was added to track the boats position and measure the sailing speed. Table 2 shows a list of the selected components and main specifications.

Table 2 - Sensor hardware specifications.

Sensor	Name	Data Rate	Communication	Power
IMU	ISM330DHCX + LIS3MDL	*<6.7kHz*	*I2C*	*3-5V*
Ultrasonic Sensor	*DFRobot A02YYUW*	*<10Hz*	*UART*	*3-5V (<8mA)*
GNSS Module	*Adafruit Ultimate GPS (99 channels)*	*<10Hz*	*UART*	*3-5V (<34mA)*

The selected sensor suite was integrated into a single architecture as shown in Figure 14. Initially, the raw measurements collected were passed through calibration scripts to improve the off-the-shelf accuracy and reliability of the data. In the case of the ultrasonic distance sensor, finding the appropriate calibration involved performing an experiment to take sample measurements at known distances, and using linear regression to find the scale factor and bias. For the IMU, the standard practices for calibration recommended by the manufacturer were applied to the accelerometer, gyroscope and magnetometer.

The calibrated measurements were then combined to provide a full estimation of the boat's states using sensor fusion techniques. This was achieved by employing an algorithm known as the Kalman filter, which takes in a physical model of a dynamic system and combines different sensor measurements into a state estimate considering each measurement's uncertainty.
This is achieved in two steps. First the system model is used to make a prediction of the state. This prediction is then corrected by direct measurements of that state through the calculation of a weighted average. The weights are estimated from the system's covariance matrix, which is essentially a measure of the prediction uncertainty. The level of trust the filter places in the model versus the measurement is commonly referred to as the Kalman filter gain [4]. The Kalman gain is calculated recursively at each step forward of the system and uses the previous state value and covariance to reinitialize the prediction.

Three separate decoupled implementations were made for the sensor package on board. Initially, the accelerometer, gyroscope and magnetometer readings were fused using an Extended Kalman Filter to estimate the boat's absolute orientation in the form of Euler angles (roll, pitch and yaw). Next, these angles were combined with the raw accelerometer measurements to calculate absolute vertical and horizontal tilt-compensated accelerations. The vertical component was then fused with the ultrasonic sensor measurements for the calculation of the foiling ride height while the horizontal component was merged with the GPS position tracking to provide an accurate measure of boat speed.

For each sensor, a driver was written in the form of a Python *class*, which included the appropriate sensor fusion calculations and was accessed by the *sensors.py* script as previously described.

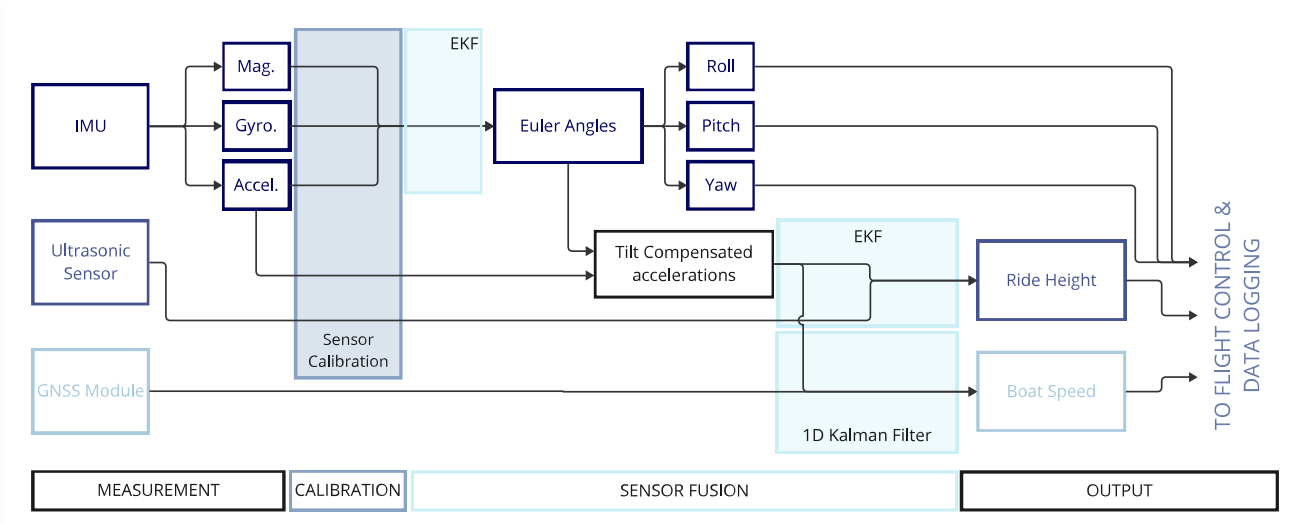

Figure 14 - Sensor package & sensor fusion architecture.

1.4.4. Telemetry

Radio communication was incorporated to the system with the aim of sending the data to shore during testing and the *SuMoth Challenge*. An RFM95x LoRa (Long Range radio) transceiver (3) enables low power telemetry capability over distances up to 5 kilometres. This was key to ensure data obtained during the limited testing time was not lost in case of water ingress.

On the shore side, an identical radio transceiver and antenna were connected to a second Raspberry Pi (the shore computer) that was responsible for decoding the radio packet and transferring it into the either a local network or the internet if provided with an adequate connection. Once in the network, the real-time dashboard presented in Figure 15 allowed the team to see the boat attitude in real time. The latter was developed using Streamlit, an open-source Python framework that supports rapid development of interactive web applications. The code interprets the structured data packets, calculates the time elapsed between packets and displays the data in various formats such as gauge, line plots and maps for GPS positioning as well as each sensor status.

Both the telemetry and the dashboard underwent range and connection stability testing to optimize transmission parameters and functionality. As part of testing, the team also identified the need for a server-deployed dashboard version, which would allow the use of phones during testing without having to risk computers getting splashed. For this reason, an option to select the hostname is also provided, allowing the team to easily switch between networks and not have to run the code locally.

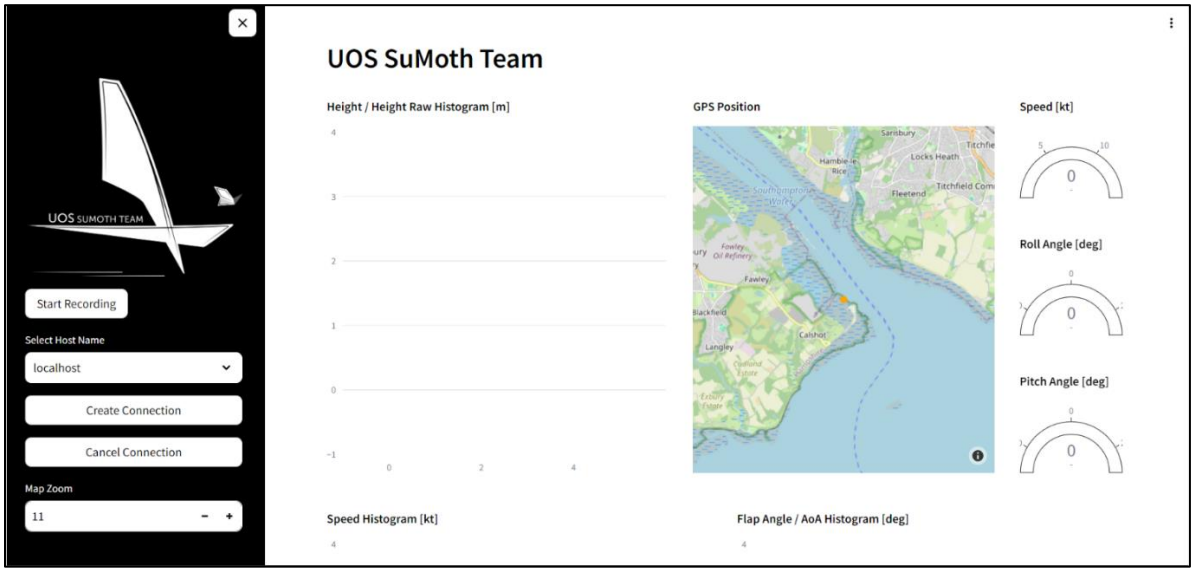

Figure 15 – Snapshot of dashboard interface.

1.4.5. Powering

A key requirement of the system was to be capable of running for the duration of a normal competition day (approximately 6hs). As shown in Figure 16, the flight computer, sensors and telemetry system are powered by a 10Ah portable power bank. This simple solution can easily support multiple power outputs and charging cycles and provides a 7-hour autonomy. For components with higher power demands, such as the servo controlling the ride height, a more robust solution was necessary. Three 14.8, 2.2Ah Li-Po batteries were connected in parallel and housed in a fireproof bag (4) to enhance safety, offering a 12-hour autonomy at a stepped down voltage (5) of 7V.

The layout of components was also strategically designed using Wago In-Line Connectors to facilitate quick disassembly and component replacement if required during tests.

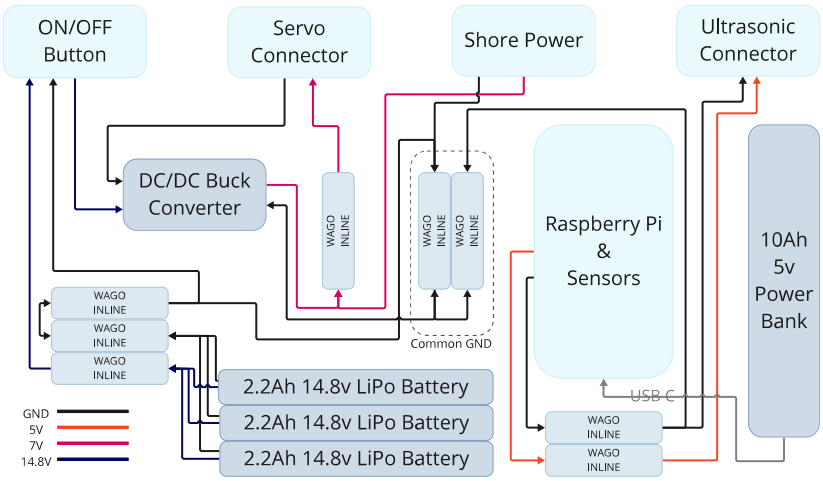

Figure 16 – Power and Connections Schematic for Data Acquisition and Control System.

1.4.6. Communication Protocol

The communication protocol plays a critical role in ensuring the seamless exchange of data between various components of the flight computer system. After evaluating several communication methods, MQTT (Message Queuing Telemetry Transport) was chosen due to its effectiveness in facilitating asynchronous communication through a publish-subscribe model. This protocol allows for efficient data distribution and real-time updates across multiple systems, which is crucial for the dynamic sailing environment.

MQTT operates with a broker-based architecture, which simplifies the integration and scaling of system components. The flight computer acts as a publisher, generating data messages categorized into topics like sensors, telemetry, logging, controller, actuation, and input. Each script within the architecture subscribes to relevant topics, maintaining high modularity and ensuring that updates or errors in one part do not disrupt the entire system.

This communication strategy enhances the robustness and flexibility of the flight computer, enabling it to adapt to additional modules and handle potential hardware failures without compromising overall functionality.

1.5. Control System

Feeding directly from the data acquisition system designed by the team, an alternative electronic ride height controller was created. On the hardware side, the *wand* system was replaced by the servo-actuated mechanism depicted in Figure 17. As seen, in the new system a pushrod connects the servo arm directly to the foil lever by means of a rod end with a ball joint. The attachment method replicates exactly that of the original wand system, as backwards compatibility was one of the main design requirements. This allows the sailor to switch back and forth between ride height control with an easy motion while out on the water during testing and racing, effectively acting as a safeguard in the case of malfunction of the flight computer. Since the servo motor is exposed to water and elements on deck, a 45kgf.cm torque IP67 waterproof servo by *DFRobot* was selected as the actuator. A wooden and flax-fibre composite mounting base was bonded to the deck and included a removeable section to allow for replacement and maintenance to the servo.

On the software side, the control approach selected was a Linear Quadratic Regulator (LQR), favoured over the common Proportional-Integral-Derivative (PID) controller. The LQR approach was chosen for its ability to efficiently manage systems around an operating point (i.e. an equilibrium state), even when faced with small deviations that are common in complex dynamic settings like sailing. This is particularly beneficial for high-speed foiling Moths, where maintaining stability and performance during transitions between different modes of operation (e.g. from displacement mode to foiling) is critical. The sailboat's interaction with varying wind speeds and water conditions also introduce significant nonlinearity in system behaviour, making the predictive and adaptive control capabilities of LQR highly suitable.

Unlike PID controllers, which primarily respond to error signals, the LQR operates based on an optimization principle that minimizes a cost function. This cost function includes terms for both the state error (with matrix Q) and control effort (with matrix R) which allow the controller to balance performance with energy expenditure and actuator activity [5]. By adjusting Q and R, the controller

can be finely tuned to prioritize certain states over others, such as minimizing pitch oscillations without overly aggressive flap movements.

As full-state controllers, LQRs require an accurate and informed model of the system dynamics to be able to operate, once again unlike their somewhat 'physics oblivious' PID counterparts. To this end, an implementation of the equations of motion governing the boat when foiling was created. An initial model based on the work by [6] was implemented for validation and further expanded to accurately represent the sailing case. Since the system was built with the aim of controlling a single action, namely the flap angle, the physics were simplified to a 2D, 3-DoF model with the vessel free in pitch (or trim), heave motion and surge. While it is acknowledged that the boat roll (or heel) motion will affect the hydrodynamics of the boat, the single continuous flap means that active roll control is beyond the capabilities of the system, and it is therefore left to the sailor's ability.

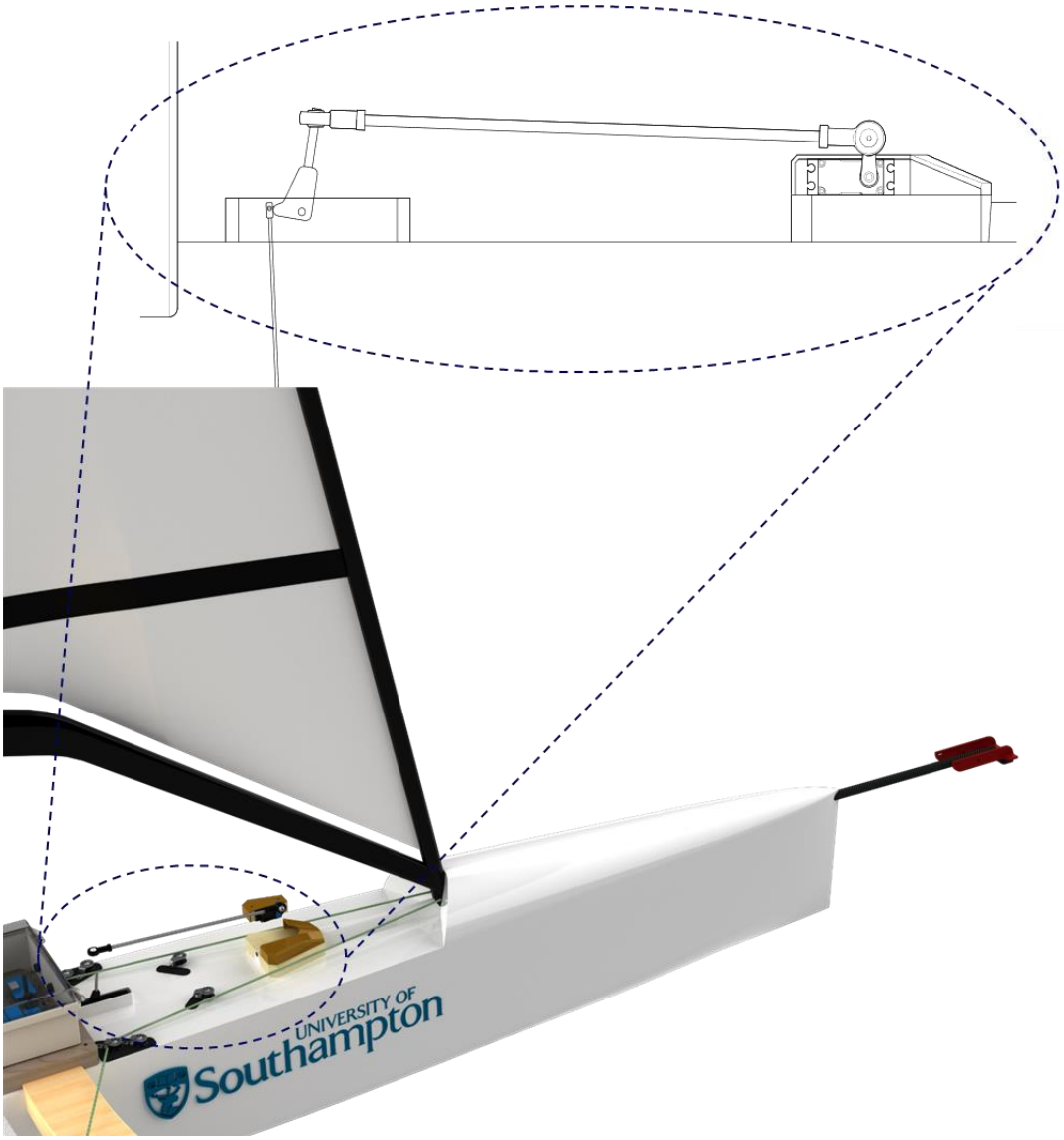

Figure 17 – Visualisation of electronic ride height control servo actuator and sensors.

1.5.1. Dynamics Model

As previously mentioned, a model of the physics governing the boat's foiling mechanics was required for the implementation of the LQR controller. The model was created as a simplification of the real sailing physics and considers only motions that happen in 2D within the XZ plane (as denoted in the diagram in Figure 18). Furthermore, the dynamic controller is only expected to be operational when the boat is already up on the foils, and therefore no buoyancy or drag forces on the hull are included in the model.

The main forces acting on the boat, as depicted in the diagram, are the lift and drag generated by the foils and the immersed portions of the verticals, as well as the boat weight and the drive force generated by the sails.

The total weight and centre of gravity (CG) of the boat was directly calculated from a broken-down table of weights and centres produced by the team. However, we must also account for the weight and position of the sailor, which can have a large influence on the position of the CG in a boat this size. Given a known sailor position, the final CG could be estimated by means of an average of the sailor and boat CGs weighted by their respective masses.

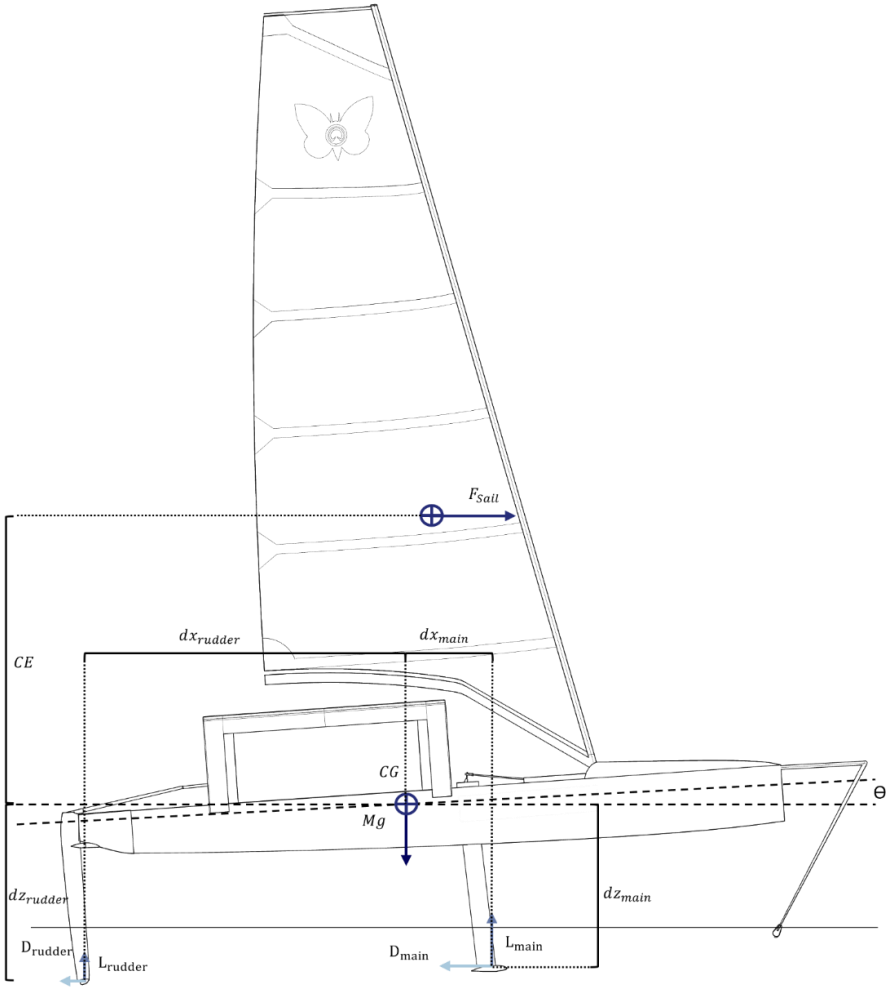

Figure 18 (right) – Diagram of foiling Moth with main forces

An initial value for the sailing drive force $F_{x,sails}$ and expected sailing speed V are fed into the model, allowing the lift and drag forces to be estimated, by the standard lift (Eq 1) and drag (Eq 2) equations for both the main foil and the rudder, as shown in below:

$$Eq\ 1\text{: } L = \frac{1}{2}\rho V^2 A C_L \qquad Eq\ 2\text{: } D = \frac{1}{2}\rho V^2 A C_D$$

The foil verticals were assumed to have an associated drag component but produce no lift. The lift and drag coefficients C_L and C_D, respectively, were obtained from the 2D interpolation of the surfaces given in the plots in Figure 19, which were built from XFLR5 analysis performed on both the baseline and the newly designed foil shapes. The angles of attack are calculated considering the boat pitch at every moment.

If we then solve for a balance of forces, considering the horizontal and vertical components of each, the heave and surge accelerations can be calculated. The resulting equations of motion are shown in Eq 3 and Eq 4:

$$Eq\ 3: w' = \frac{M\ g\ \cos\theta - L_{rudder}\cos\theta - D_{rudder}\sin\theta - L_{main}\cos\theta - D_{main}\sin\theta}{M}$$

$$Eq\ 4: u' = \frac{F_{sail} + L_{rudder}\sin\theta - D_{rudder}\cos\theta + L_{main}\sin\theta - D_{main}\cos\theta - Mg\sin(\theta)}{M}$$

Similarly, taking moments about the overall CG allows us to calculate the pitching motion acceleration, defined as:

$$Eq\ 5: \theta' = \frac{1}{I_{yy}}(dz_{main}\ L_{main}\sin\theta + dx_{main}L_{main}\cos\theta - dz_{main}D_{main}\cos\theta + dx_{main}D_{main}\sin + dz_{rudder}L_{rudder}\sin\theta - dx_{rudder}L_{rudder}\cos\theta - dz_{rudder}D_{rudder}\cos\theta - dx_{rudder}D_{rudder}\sin\theta - F_{sail} * CE)$$

Note that here the drag values already include the drag from the verticals.

If we then integrate these values and use a transformation matrix to transform the components of velocity and acceleration from the pitched boat axis to the inertial world axis system, we can obtain the vessels pitch, forward travel speed and ride height. The estimated states of the hydrofoil boat can then be summarized as in the vector x below, with θ the boat pitch, $\dot{\theta}$ the pitch rotational speed, u the surge velocity, w the heave velocity and z the boat's ride height.

$$Eq\ 6: \boldsymbol{x} = [\theta\ \dot{\theta}\ u\ w\ z]$$

With the system inputs given as:

$$Eq\ 7: \boldsymbol{u} = [\alpha_{main}\ \alpha_{rudder}\ F_{sail}]$$

α_{main} and α_{rudder} the main foil flap angle and rudder position, respectively, and F_{sail} sail drive force. These state values are then fed back into the system, which once again calculated the balance of forces and updates the states once again. As shall be shown in the next section, the LQR controller implementation uses a MATLAB Simulink linearization of the current system to calculate the optimal main flap angle.

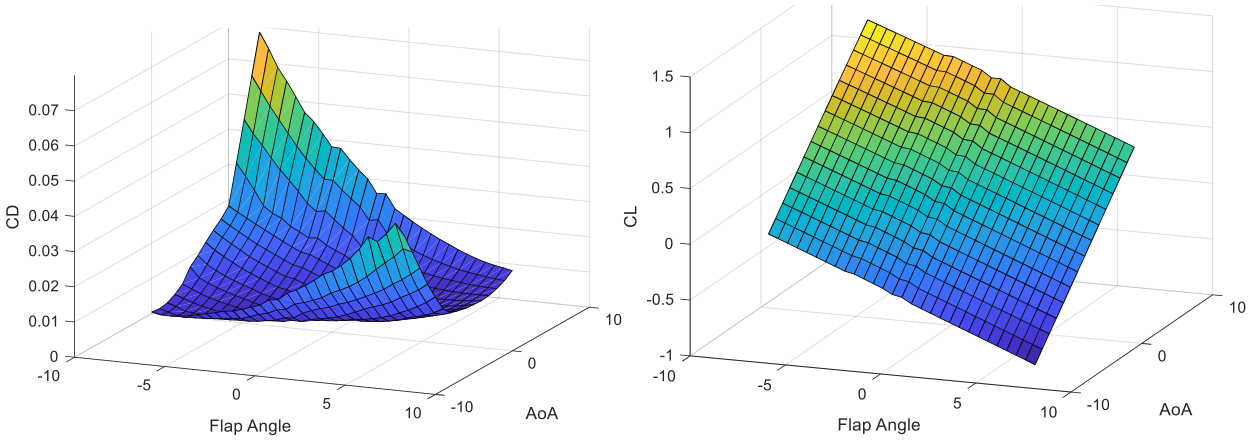

Figure 19 - Surface plots of Lift (left) and Drag (right) coefficients.

1.5.2. Controller Design & Tuning

Leveraging the dynamics model, MATLAB Simulink was also used to design the LQR controller. A few modifications to the common controller were required in order to successfully control the boat ride height. Firstly, integral action was included to remove the bias error in the output response. This was also combined with delta implementation by moving the integrator block, therefore not only integrating the error signal and saturation but also all other feedbacks [5]. Combined, these modifications were key to remove the oscillations experienced in the flap angle response when the controller was initiated.

Additionally, preliminary controller testing showed the necessity for anti-windup implementation as unexpected behaviour was observed close to the maximum set angles for servo actuation. This was determined to be an effect caused by the integrator continuing to accumulate error as it tried to push the system past its physical limits. To address this issue, the discrepancy between the signal before and after the saturation block was fed back into the integrator, effectively pausing the integration process until the input returned within an acceptable range, resulting in the controller presented in Figure 22.

For our application, the Q matrix was configured to heavily penalize deviations from desired ride heights and pitch angles, which are critical for maintaining the boat's stability and dynamic performance. This penalization was calibrated using Bryson's method [7], where each matrix entry was sized according to Eq 8 and the expected ranges of each state variable described in Table 3.

$$Eq\ 8: q_j = \frac{1}{X_{RANGE}}$$

For the R matrix, the step responses of the non-linear system were investigated for a range of *R* values as shown in Figure 20. It was found that large values of R made the system too reactive and led to overshoot, therefore a value of *R=0.1* was selected yielding a controller response of approximately 5 seconds, which is comparable to the mechanical wand actuation.

Table 3 – Ranges for Q Matrix estimation using Bryson' method.

State	Min	Max	Range
θ [deg]	-15	15	30
$\dot{\theta}$ [deg/s]	-10	10	20
u [m/s]	5	13	8
w [m/s]	-1	1	2
z [m]	-0.2	-1	0.8

A single set of gains was not sufficient to control the Moth across the common range of speeds. For this reason, gain scheduling, an approach where the controller dynamically adjusts the gains based on real-time changes in system behaviour [8], was implemented. Four different sailing scenarios were modelled using the non-linear dynamics: take-off, upwind sailing at 7.5 and 10 ms^{-1}, and downwind at 12 ms^{-1}. Variations such as the position of the sailor on the boat, shifting the centre-of-gravity aft for take-off and downwind to help control the pitch, as well as different rudder angle configurations were also considered. For each sailing condition, MATLAB's Model Linearizer tool was used to obtain the state-space representation of each operating point.

The integrator gains were computed by solving the Ricatti equation [9] using MATLAB's *"lqr"* function for the extended system (including integrator) in Eq 9 and observing the system response to a heave step input for different values of q_i in the matrix *Qi* (Eq 10). The different responses are presented in Figure 21, which shows that for a value of q_i = 10 there is already unwanted overshoot. For this reason, q_i = *1* was selected for all sailing cases, and a similar process was then used to vary define the K_{sat} constant which was defined as K_{sat} = 1 to prevent oscillations.

Eq 9: $$\begin{bmatrix}\dot{\boldsymbol{x}}\\ \dot{x}_i\end{bmatrix} = \begin{bmatrix}A & \mathbf{0}\\ -C & 0\end{bmatrix}\begin{bmatrix}\boldsymbol{x}\\ x_i\end{bmatrix} + \begin{bmatrix}B\\ 0\end{bmatrix}u + \begin{bmatrix}\mathbf{0}\\ 1\end{bmatrix}ref$$

Eq 10: $$Q_i = \begin{bmatrix}Q & \mathbf{0}\\ \mathbf{0} & q_i\end{bmatrix}$$

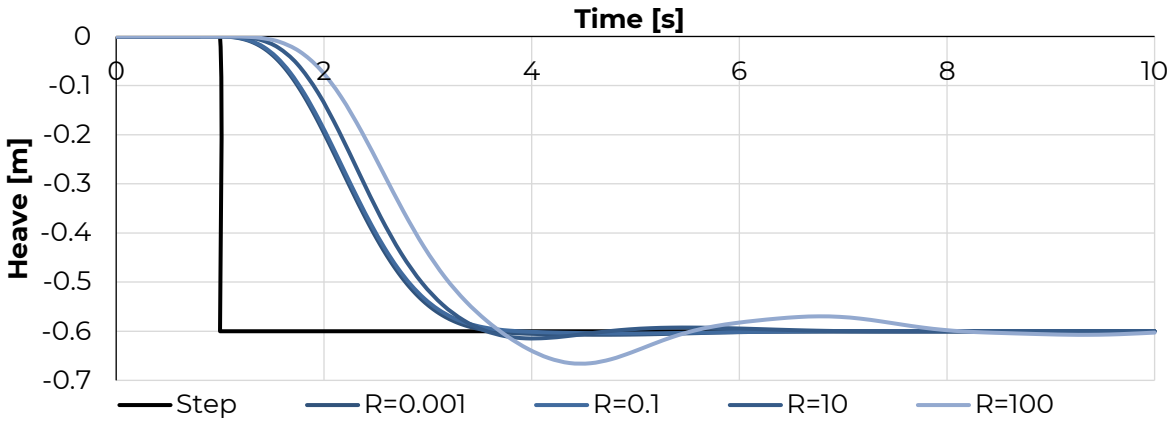

Figure 20 – Main foil step with LQR control for multiple R values.

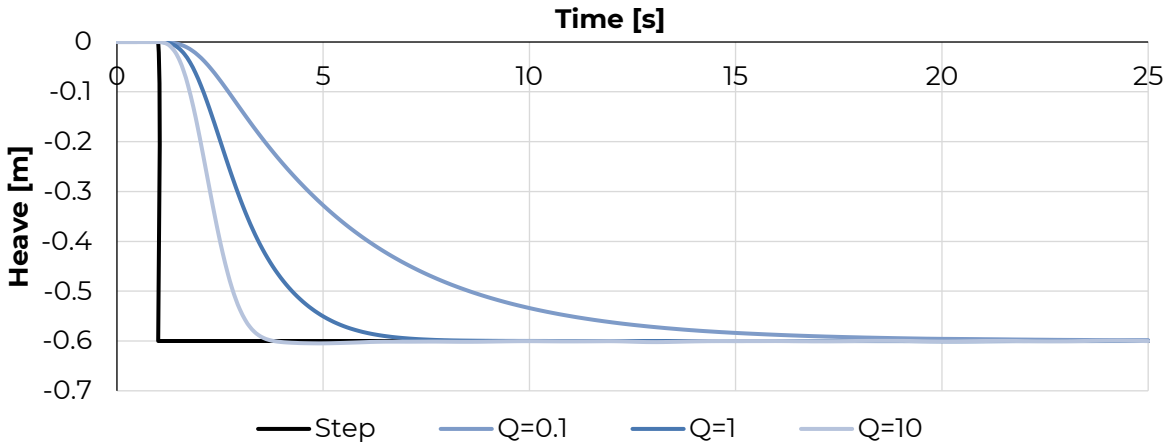

Figure 21 – Main foil step with LQR control for multiple q_i values in the extended Qi matrix

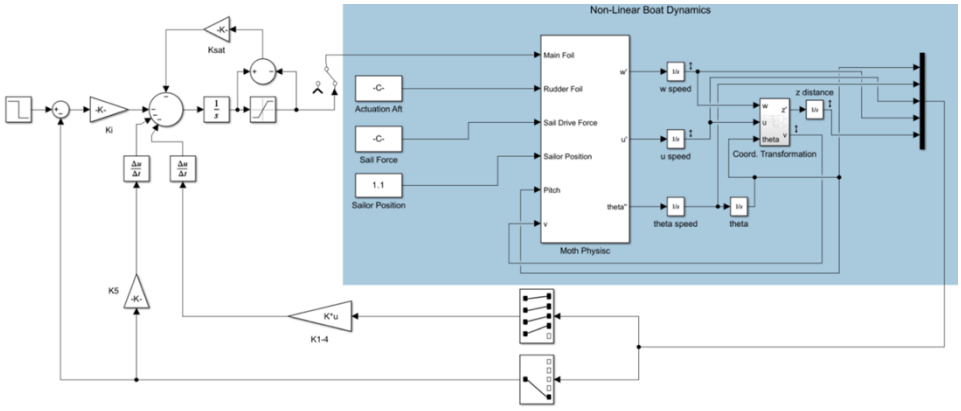

Figure 22 – LQR controller design in MATLAB Simulink.

2. MANUFACTURING AND COST ANALYSIS

2.1. General Description

As previously discussed, working from the legacy left by the previous 2022 UoS SuMoth in the form of a solid platform consisting of the flax infused hull and wooden wingbars, this year the team decided to focus on the main hydrofoil horizontal as well as the ride height control system. The hull was received by the team in good condition and only minor maintenance was required, as was the case with the rig. The manufacturing plan for the newly redesigned hydrofoil was informed along the way by the MS360 sustainability analysis, which helped identify the elements in the part's lifecycle with the highest impact, as well as the ones with the highest space for improvement. The main horizontal manufacturing procedure taken is detailed in the section below.

2.2. Testing for Manufacture

Orienting the manufacture of our foil toward sustainability and with our small experience of manufacturing, it was crucial to thoroughly test our manufacturing ideas. The foil was designed with the goal in mind that it had to be manufacturable. For our only prototype to meet our design criteria and be manufactured, all the processes used had to be trialled and mastered before the manufacture of the final foil design could begin.

2.2.1. Material Selection

After researching and drafting the processes involved in our foil manufacture, it was decided to opt for carbon and flax fibres for the foil structure. Carbon was picked due to its lightweight nature and strength. Gurit SE75 prepreg carbon was selected thanks to our partner, Carrington Boats who offered us the material after initial contact. The possibility of using their off cuts from racing yacht manufacturing was offered for our project free of charge. The use of such a material would not have been financially viable otherwise. The choice of using flax fibre was driven by its sustainable nature and a rule within the *SuMoth Challenge* requiring the foil to have a maximum of 60% of carbon as its total weight. This limitation prevented the team from using less dense sustainable material for our manufacture such as wood. Both materials were tested to confirm their manufacturing process.

2.2.2. Hinge Material

The main feature differentiating a moth foil from most commercially available foils is the presence of a flap which enables the control of the foil's lift and Moth ride height. A robust solution must be found to connect the flap to the main wing while allowing its rotation about the hinge. There are two main methods commonly used in the industry, the use of a Kevlar strip embedded in the laminate or the use of Sika 291, a flexible marine sealant and adhesive. The first solution was selected as it was recommended by Maguire Boats, one of the world leaders in Moth manufacturing during one of our consultative meetings. Additionally, a 3m strip of the hinge material they use on their own foils was donated to us to test and use on the final design. As shown in Figure 23, the 40mm wide Kevlar strip was embedded withing the laminate of two 3mm thick quasi-isotropic carbon plates, spaced 4mm apart to test it. The test was conclusive, showing the Kevlar hinge enabled approximately 20° of decoupled motion.

2.2.3. Choice of Mould Material

From previous manufacturing experience and according to the LCA investigation, it was apparent that the mould would be the most crucial part of the sustainability impact. The latter also needed to be shaped accurately to allow the final manufactured product to be as close as possible to the final design while being reusable. In industry, aluminium or tooling boards are typically used, these were the materials proposed to us by the university and used by Maguire Boats on their foils. However, these materials generate high levels of equivalent emissions and energy use as explained in the LCA analysis, therefore they do not satisfy our aim of improving the sustainability of foil manufacturing.

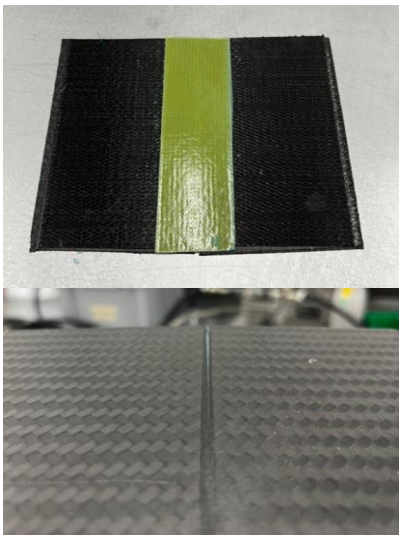

Figure 23 - Trial of Kevlar hinge between carbon plates

After brainstorming ideas, discussing and researching, wood timber was selected as the most promising solution. It is machinable, inexpensive and easy to source. However, doubts remained regarding the materials ability to perform at the high temperatures experienced during the pre-preg curing process.

A second material, hailed for its sustainability and reusable nature was plaster. It has good heat resistance properties and could be reshaped into any design. However, it requires a master mould to obtain the required shape. Adding an extra layer to our manufacturing process.

Both solutions were tested, and the result is shown on Figure 24. The wood mould was machined from a pine beam in average condition, already presenting a few cracks; a worst-case scenario. The machining worsened these defects, however sealing the wood surface using epoxy resin mitigated this issue. The seal assured a good finish and enabled the part to be easily removed from the mould. The plaster mould was shaped using a 3D printed foil section and covered using vinyl. Both were cured according to Gurit's recommended processes and came out of the oven in good condition and with the required shapes. The wood mould did not warp any further as the lowest heat setting was used during the curing process. However, the plaster mould became brittle during cure and cracked as the part was demoulded. Ultimately, wood was selected as our final mould material due to its improved sustainability and robustness compared to plaster. The use of plaster could be recommended over wood for single use moulds with complex geometry, smaller parts and quick prototyping.

Figure 24 - Trial of plaster and wood mould

2.3. Design for Manufacturing, Processes and Mould

From our testing and using the conclusion of the work carried out by the LCA, structures and performance design, the team was able to come up with the foil lay-up shown in Figure 25. Using the foil model and slowly iterating between multiple foil designs, the carbon content was optimised and the right laminate thickness was calculated. The top laminate shown in purple (0° UD ply), blue (woven ±45° ply) and green (woven 0/90° ply) shows how we have chosen the top skin containing the Kevlar strip making up the hinge of the flap to be only made of pre-preg carbon. While the lay-up on the main wing follows the thickness for the required stiffness, the lay-up has been reduced on the flap. The carbon present on the flap assures the Kevlar hinge will stay in place. Only the skins of the main wing were made from carbon, while the rest of the foil, its core and the lower section of the flap were made using flax fibres which were wet laminated

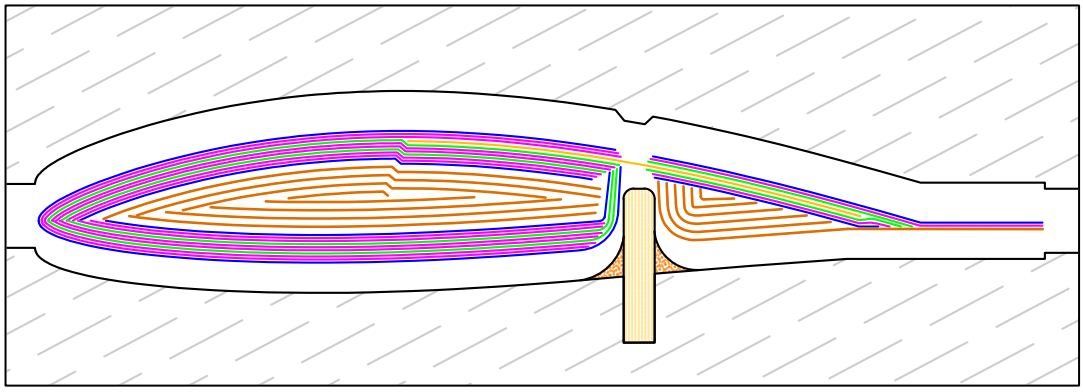

Figure 25 - Side view of mould and foil layups at root of wing.

2.3.1. Foil Manufacturing Process

The first step of the manufacturing process was to lay the plies of both skins on the mould with care, following our laminate plans. The pre-preg was cured using an oven at 80°C. Post cure, the cured skins were demoulded, and the moulds were assessed and repairs made if needed. Using the moulds, the skin leading edges and laminate on the trailing edge were surfaced (not trimmed) to allow both skins to lie flush against one another at their point of contact. With both skins surfaced, the flax plies were carefully added to the inside of both skins to make up its core and applied on the bottom skin mould aft of the hinge insert. Bio-epoxy resin was added to the flax fibres and the foil was closed, both skins clamped against one another (the moulds can be used for that operation). The flap was then clamped down against the bottom skin mould such that the flax plies of the lower section adhered perfectly to the carbon of the top section. With the foil closed and flap fully built, the trailing and leading edges were trimmed. The foil surface was smoothed down and an epoxy coating was added. Sika was added on both sides of the Kevlar hinge to protect it, the mast insert was drilled, and a metal insert was added to flap to ensure that the foil could connect to the foil mast and the flap controlled by the foil system.

2.3.2. Influence of Manufacture on Design

From a manufacturing standpoint, the design of the foil had to enable the feasibility of this makeup and the presence of the mast insert in the fuselage shown in Figure 26. Consequently, the design of the fuselage became solely driven by manufacturing, an aero section was picked, and its dimension altered to enable the mast insert to be fully fitted within it. Careful iterations had to be completed as the mast insert laminate (the prepreg plies applied around it) could not interfere with the lower skin laminate as the bottom of the mast connection sits close to the lower skin.

The hinge gap is another feature which was driven by manufacture. Its dimensions were dictated by the mould material limitations, as we ultimately opted for a 3 mm thick plywood strip to be added to the mould after machining to act as the hinge insert. The insert dimensions were limited to the strip dimensions. Owing to the hinge presence, high foil stiffness was required to allow it to work under load. Another benefit of the flat hinge was also the ease of manufacture. Due to this constraint, features such as dihedral could not be included in the design. A thicker foil section was appreciated for manufacturing purposes to optimise the carbon content while maximising the use of flax fibres.

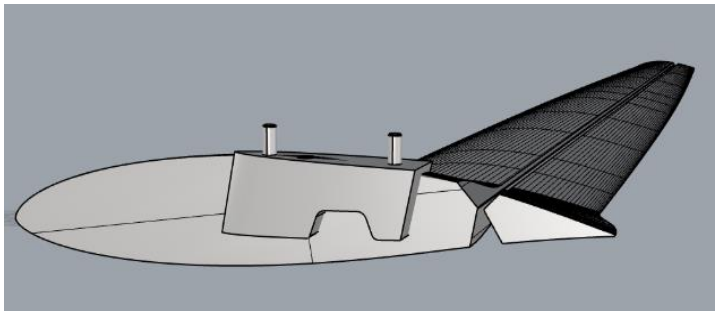

Figure 26 - View of mast insert in fuselage.

Figure 27 - Final mould lower skin with hinge insert.

2.3.3. Final Mould

The mould model was completed immediately after the final foil design was completed. The pine timber to be machined had been sourced weeks prior. The model was sent to the machining centre at the university and within a week the mould was completed. Due to a subpar result from the machining, caused by a combination of complex geometry, issues with programming the CNC machine and material limitations, the mould had to be finished by hand. Defects were sanded down or filled with wood sealant. The hinge insert and filets were also added on either side. Bio-epoxy laminating resin was used to seal the surface of the mould, allowing for a good foil surface finish, easy demoulding and for a vacuum to be created on the prepreg plies directly on the mould. This is a requirement to use prepreg carbon.

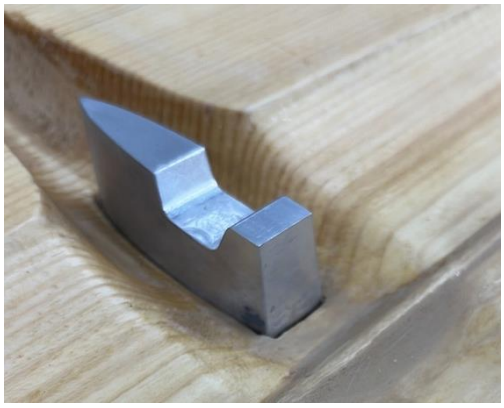

Figure 28 - Mast insert in mould on top skin mould.

2.4. Materials

The final selected materials selected are:

- Gurit SE75 carbon prepreg : off-cuts from Carrington Boats out of shelf life. They enable a high stiffness for the foil. The fibre weight is either 200g or 300g, woven or UD. It used for the main wing skin and flap upper surface.
- Biax flax 360g : provides reinforcement for the foil, driving down our use of carbon, it used for the foil core and flap.
- Easy composites LB2 bio-laminating resin : Used for laminating the dry flax fibres.
- Kevlar strip 45mm x 400g/m^2 : Used for the foil hinge and embedded between the main wing and flap top skins.
- Easy composite XCR Coating Resin : Enables a clear finish for the surface of the foil, fills the imperfection such as pin holes on the prepreg skins and provides a layer of UV resistance to our foil for a more durable product.
- Sika 291i : Flexible silicon compound supporting the Kevlar to ensure the durability and good operation of the flap hinge.

2.5. Costing

As the only cost change between our original vessel and our current relates to the Vessels appendage. Our costing will start with the previous vessels costing before showing the new appendages costing.

Previous Vessel Costing

This Table relates to our 2022 SuMoth Project

Part	Cost in $SM
Hull	1037.05
Wing	126.50
Appendages	1172.15
Rig	2699.24
Control System	342.5
Total	5377.43

Previous Group Appendage Cost with New Rules

This is the previous costs with updated rules and costings.

Part	Composition	Year made	Design year	Cost in $SM
Rudder horizontal	Pro	Pre 2012	Pre 2012	500
Rudder vertical	Pro	Pre 2012	Pre 2012	1500
Main horizontal	Pro	Pre 2012	Pre 2012	500
Main vertical	Pro	2022	Pre 2012	1500
Total				4000

New Main Foil Horizontal Cost

Material	Quantity	Cost in $SM
Recycled prepreg CF HM	0.391 kg	146.64
Flax	0.1584 kg	0
Bio Epoxy resin	0.18 kg	2.7
Kevlar	0.0288 kg	3.456
Wood	31.8 kg	0
Sikaflex	0.0455 kg	1.1375
CNC machining	6 hrs	240
Oven Curing	8 hrs	160
Consumables		
Breather	1	3
Vacuum bag	4	8
Spiral Tubing	1	1
Tacky tape	6	3.2
Release agent	0.01	1
Total		470.13

New Appendage Cost

Part	Composition	Year Made	Design Year	Cost in $SM
Rudder Horizontal	Pro	Pre 2015	Pre 2015	500
Rudder Vertical	Pro	Pre 2015	Pre 2015	1500
Main Horizontal	Self-Made	2024	2024	470.13
Main Vertical	Pro	2022	Pre 2015	1500
Total				3970.13

New Total Cost

Resulting costing from the production of a main hydrofoil.

Part	Cost in $SM
Hull	1037.05
Wing	126.50
Appendages	3970.13
Rig	2699.24
Control System	342.5
Total	8175.41

3. SUSTAINABILITY ANALYSIS

3.1. General description

The reuse of the legacy platform left by the 2022 team was a very early choice in the project, in keeping with the sustainability philosophy of the team. The goal is to in every entry, increase the amount of components on the boat that were fully produced by the team, and to maintain the previous components so that the boat remains safe and performant.

The chosen component to be manufactured by the team for this year's entry was the main hydrofoil horizontal. It was selected due to its critical aspect on the boat's performance as well as the high complexity of design and manufacture, with strict requirements for the hydrodynamic, structural and production aspects of its creation. The full lifecycle of the production of the foil was considered to allow the team to target the areas with the highest potential for improvement, not focusing only on the material that directly goes into the part itself but also on all the consumables and external materials that are necessary to the build.

3.2. Boat and Elements Lifecycle

The boat is intended to be used for further projects at the University of Southampton and through regular maintenance and good upkeep of the boat it will have a long lifetime. However, the end life of the boat has also been considered. Commatposites are difficult to recycle compared to other materials. Usually, the resin can be separated from the composite part through using pyrolysis or solvolysis. For our SuMoth there are concerns with using pyrolysis and the flammability of flax fibres during the process. However, the PET core would decompose at the high temperatures during pyrolysis meaning that it can be separated from the flax. Therefore, to recycle the hull the paint will be stripped off and then the parts of the hull with cork core will be separated from the parts with PET core. The sections with cork core are the foredeck, V-shaped bulkhead, bow of the hull and a small section around the centreboard case.

Pyrolysis will be used to recycle all the secondary carbon parts, foils and mast. This will separate the resin from the carbon allowing for this to be recycled. The sail could be upcycled in the future through turning it into accessories including bags and wallets. The wingbars which are built out of wood and bonded with bio-resin are coated in varnish making them challenging to recycle or upcycle. Burning the wood releases harmful chemicals from the varnish making this an unsuitable choice. The varnish can be removed by sanding off the outer layer around the wingbars and then they can be grinded and compressed for future projects where the material properties are less important such as for furniture.

Control system components can be easily reused as the system has modular aspects and components can therefore easily be removed and reused or recycled.

3.3. Foils

Composite recycling techniques described above can also be utilised for the foils. The foils are intended for reuse by further projects until their failure. Upon failure they can be recycled or repaired.

3.4. Materials

Table 4 - Emission values of studied materials.

Material	CO_2 Produced through manufacture (kg $C0_2$eq/kg)
Glass Fibre [10]	2.0
Flax Fibre [11]	0.349
Dry Carbon [12]	24.0
Prepreg Carbon [13]	53.6
Bio-resin [14]	4.1

Flax fibres produce the lowest CO_2 emissions during production as seen in Table 4, the majority of emissions originating from the harvesting of flax and processing to make the fibres. The flax crop does not require irrigation [15] which is beneficial in water scarce areas; however, it is an agrochemical intensive crop which requires extensive use of fertilisers (the production of which is energy intensive) [16] which can lead to eutrophication and acid rain. Despite this the CO_2 emissions of flax fibre are orders of magnitude lower than the other materials. And while it requires land and fertilisers to produce, for the small amount of material that we require, this would be negligible. Flax fibre composites can be recycled in the same ways as glass and carbon fibre, with the notable exception that the flax fibres can be fully incinerated, and the energy recovered. Therefore, flax fibre has the potential to be carbon neutral, and can be disposed of more easily.

Prepreg carbon consists of pre-impregnated carbon fibres and a partially cured epoxy matrix. This curing process is where the majority of the CO_2 emissions originate and the reason why prepreg has such high emissions [13]. Similarly to dry carbon, this value can be reduced through recycling in the same methods outlined for glass fibres. Furthermore, the value obtained for prepreg carbon assumes a transport distance of ~3000km unlike the other materials. Therefore, it can be assumed that the value would be slightly lower than 53.6 although still higher than the sum emissions of the base materials which are dry carbon and epoxy resin.

Bio-resin was the only matrix considered for manufacturing purposes due to the ability to attain carbon neutrality and its availability at The University of Southampton. Bio-resins are manufactured using biological sources such as vegetable oil instead of petrochemicals [17]. Therefore, they can be more sustainable than a regular epoxy resin matrix. Bio-resin has been widely observed to have a lower carbon footprint than petrol-based resins. It is widely available as a resource for other projects at The University of Southampton and therefore, waste utilisation factor can be minimised by obtaining unused resin. Table 4 clearly shows that dry carbon and prepreg produce significantly more emissions during manufacture than the other materials analysed. Therefore, it would be prudent from a sustainability point of view to limit the utilisation of these materials as far as structural integrity will allow and push the use of other materials. The information gained from the literature review clearly shows that, from a sustainability perspective, flax fibre is the most lucrative. Its manufacture results in the lowest CO_2 emissions and it can be recycled in the same methods as the other fibre options with the addition of complete incineration of the composite. The recycling options available, as well as the ability of the flax fibres to be incinerated improve the ease of disposal aspect of flax fibres. Furthermore, it can be farmed sustainably which theoretically can achieve a carbon-neutral lifecycle. Flax fibre can be used in the same manufacturing processes as carbon and can be easily obtained from composite manufacturers, indicating they are on a parity with dry carbon in terms of social sustainability. Flax prepreg is generally cheaper than the carbon equivalent

from composite manufacturers and is therefore more economically sustainable. The results of this investigation were used to prove that, from a sustainability perspective, the flax content of the foil should be maximised. Consequently, the decision was made to include as much flax in the foil as was allowed under the SuMoth regulations. It was noted that without these regulations, more flax could have been included in the final lay-up, reducing the carbon content of the foil. For our project, the SuMoth regulations were working against sustainability, for a sustainability focused competition this was disappointing, and this feedback was passed on to the competition organisers.

3.5. Actions for a sustainable future

Bio-based materials such as wood, flax and bioresin utilised in this project are one of the easiest ways to reduce the environmental footprint from the traditional composites. However, the increase in demand for bio-based materials could leads to other environmental and social issues as outlined above. Although they can absorb significant amount of CO2 during their lifetime, increase logging activities could lead to mass deforestation and loss of habitat for wild animals. The effort of regrowing trees would take many years to happen. Farming bio based materials could results in increase fertilisers used, increasing the impact of eutrophication. It could also lead to the increase in land used and potentially compete with the farming of food crops.

Reducing the use of materials is the best way to reduce the environmental footprint, by replacing a product before its service lifetime creates unnecessary need for material usage and disposal. Prioritising the use of recycling waste materials would promote circular economy and reducing the environmental burden for end-of-life treatments and the dependency on natural resources. When it is not possible to use recycled materials, choosing bio-based materials over non-bio-based materials whenever possible. Collaboration between industry leaders is important to ensure the environmental and economical sustainability of the industry. Improving the sustainability of the industry will facilitate the future proofing of the industry, allowing future innovation.

4. TEAM

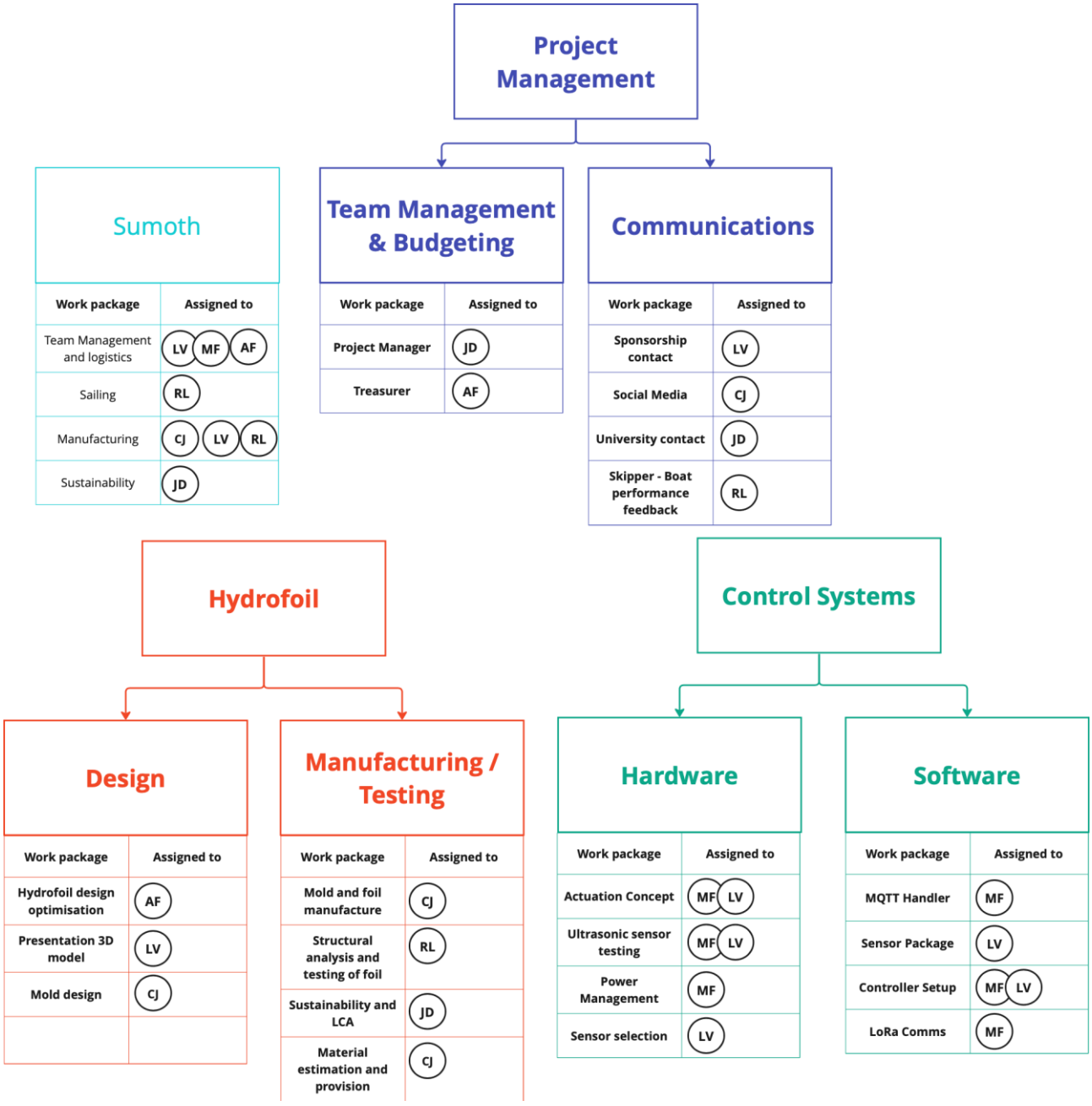

Figure 29 - Team Structure

4.1. TEAM MEMBERS

- *Leonardo Vassimon*

With a background naval architecture and experience in wooden/composite boatbuilding and a love for making things, Leo (originally from São Paulo, Brazil) was chosen as Team Captain for this edition of the SuMoth. His versatile previous work enabled him to create good communication between the two main areas of the project: control systems and foil design and manufacture, to make sure that everything would fit together in the end, he also took direct action in the development of the foil manufacturing plan, and in the creation of the data acquisition sensor package as well as the design of the electronic ride height controller.

- *Matias Figueiras*

Matias was selected as Team Co-Captain to assist Leo on the overall project management. On the technical side, he leveraged his coding and performance simulations experience as the control systems lead, working on the development of the data telemetry system and flight computer architecture. Furthermore, he was responsible for integrating the boat dynamics model with the LQR controller as well as carrying out improvements and tuning of the during in-land and sailing tests.

- *Corentin Jego*

CJ as head of manufacturing and communications, thoroughly planned and executed the manufacture of our new hydrofoil. With a background in aerospace engineering, sailing and boat building, he was able to improve all of his skills during this arduous task. Developing a brand-new hydrofoil design, manufacturing it with limited resources and time was definitely a challenge, yet it was one that we completed successfully. He can't wait to compete with this new foil in Garda.

- *Adam Fermor*

As Performance design lead, Adam was in charge of the foil design optimisation building upon his naval architect experience while expanding his knowledge on machine learning , developing from scratch, a novel generative adversarial network to generate new foil designs . This machine learning approach was essential in developing the foil design along with regression analysis. Currently he alongside the entire team is eagerly waiting to put our foil to test in Garda.

- *Jack Durston*

As the team member in charge of sustainability Jack ensured that materials and time spent manufacturing were tracked throughout the project. In addition to utilising Marineshift360 software to assess the sustainability of our project in terms of environmental, social and economic sustainability.

- *Rhys Lewis*

Rhys led the structural design aspect of the project, closely working with the manufacturing and performance teams to ensure that reducing the CFRP content of the foil did not sacrifice stiffness, through changes to the section and planform shape and optimising the laminate layout. Additionally, Rhys led all sailing operations throughout the project.

5. MARINESHIFT 360 LCA

5.1. General results

The LCA was completed in Marineshift360, using records kept by the manufacturing team for material usage and hours spent manufacturing. The results of the LCA are illustrated in, Figure 30, Figure 31 and Figure 32. Figure 30 and Figure 31 show a breakdown of CO2 emissions (kg CO2eq) and energy consumption (MJ) respectively. The control system is the highest contributor to emissions followed by sample and part manufacture. As previously stated, the estimate for the emission contribution of the control system is likely to be an overestimate due to basing the estimate off LCAs completed for commercial laptops, which include materials such as screens and metal casings. Figure 31 shows that the samples were the main contributor to energy consumption, followed by the control system and part manufacture.

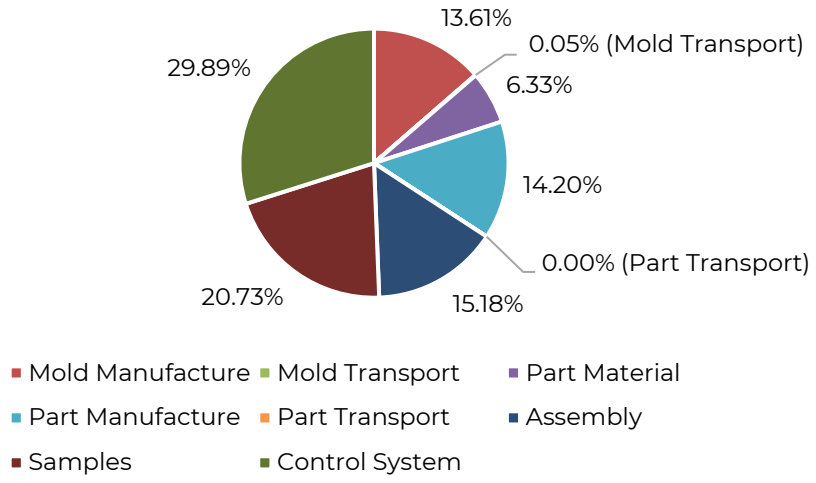

Figure 30 - Final LCA global warming emissions breakdown.

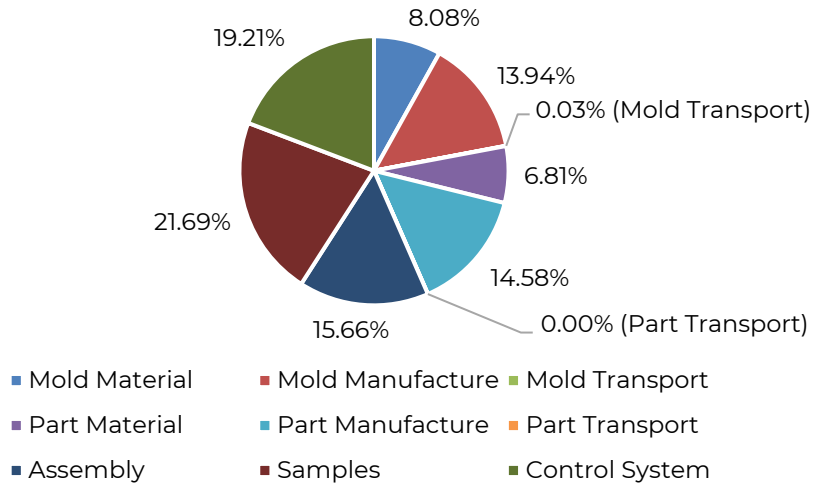

Figure 31 - Final LCA energy consumption breakdown.

The use of wood produces a negative CO2 emission due to the CO2 absorbed by the material during its growth. The reduction in emissions and energy consumption due to the changing of the mould material can also be seen in Figure 32. Our foil can be seen to have a mere 5.70% and 16.17% of the emissions and energy consumption respectively of the original foil. This improvement was expected after researching the sustainability impacts of the materials used and completing the mould comparison. Furthermore, many of the materials used, excluding the wood, were upcycled and destined for landfill. This reduced the waste generated in our project, giving a higher utilisation factor of 66.09% compared to 30.42%, where the utilisation factor is defined as final material divided by the ordered material. An important consideration in terms of sustainability is the ability to re-use our mould to manufacture future foils if required. The durability of a timber mould is worse than the durability of an aluminium mould. Consequently, we have found that during the finishing and manufacturing processes the mould can be damaged.

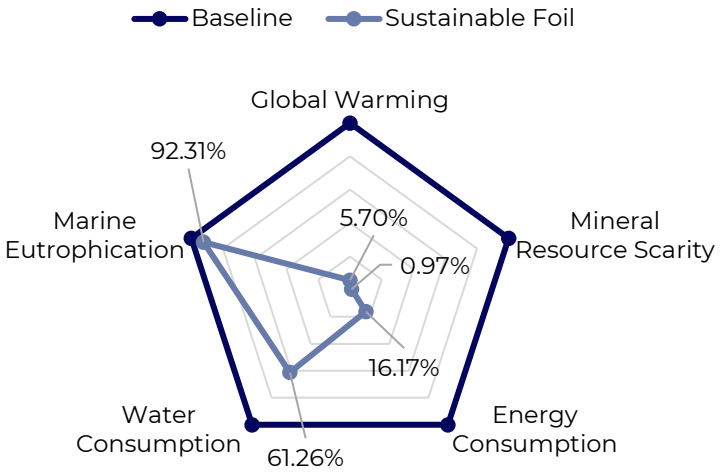

Figure 32 – Project LCA comparison to baseline.

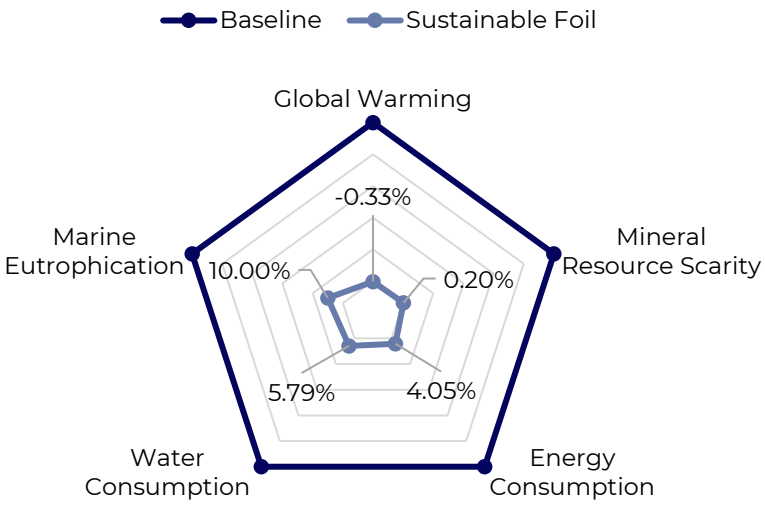

Figure 33 - Comparison of new build mould to baseline mould.

Results showed that 17 moulds and foils could be manufactured before the emissions exceeded that of an aluminium mould. These numbers would increase if multiple foils can be manufactured from a single wooden mould. However, this does not account for the extra time of making multiple moulds. Therefore, it can be concluded that wooden moulds are more suitable for bespoke parts, such as our foil. Whereas an aluminium mould would be more sustainable for batch or mass production.

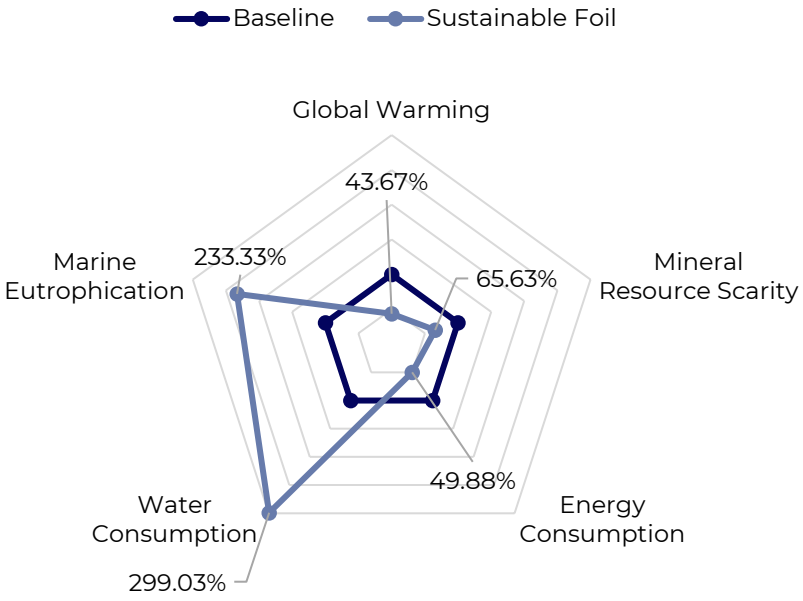

Figure 34 - Comparison of new build foil to baseline foil.

Through the investigation into potential areas which could be improved in terms of sustainability, it was identified that the mould and foil materials were critical areas which heavily impacted the sustainability of the project. Using timber as a mould material and reducing the carbon content of the foil to include flax would likely provide significant gains in terms of environmental sustainability. The individual sustainability improvements made using timber and flax can be seen in Figure 33 and Figure 34 which illustrate the difference between the moulds and foils respectively for our project and the baseline. Large reductions in global warming emissions and energy consumption as predicted through our research and investigation have been observed. An increase in water consumption and marine eutrophication is shown in Figure 65 due to the cultivation of flax fibre and release of fertilisers into water sources, which was also predicted.

Social and Economic sustainability

Several aspects of the design choices impact the overall social sustainability of the project. Throughout the execution of the project, the team have strived to utilise upcycled and re-used materials. This includes prepreg carbon, flax fibre, manufacturing consumables, batteries, the Raspberry Pi and others. This pursuit facilitated the acquisition of high-end materials which would otherwise be inaccessible, the practice also encourages amateur boat builders to find cheap/free materials, making the sport more accessible. Furthermore, it encourages larger manufacturers to save scrap materials for distribution to projects such as ours, reducing waste in the industry. The innovative control system improves the sailor's control over the boat and allows for easier set-up of

the boat for sailing as the mechanically complicated wand system does not have to be used. Throughout the project, the team has maintained a presence on the social media platform Instagram. This has served to encourage others to develop an interest in the project and its future iterations, securing future innovation in the industry.

However, several concerns have been raised surrounding social sustainability. The increased water consumption over the baseline assessment that the project has incurred could have negative implications. If the flax and timber used in the project was grown in an area with limited water supply, then the increased water consumption of the project could increase strain on water resources in the area for applications such as drinking and cultivating food crops. Furthermore, while the timber is known to have been grown under PEFC, a UK-based sustainable growing scheme, the growing condition of the flax is unknown. Therefore, there is the possibility that sustainable farming and labour practices were not followed during its cultivation. Finally, the equipment used during manufacturing such as CNC machines, ovens and resin infusion equipment is expensive and not accessible to all manufacturers.

To conclude the sustainability assessment of the project, its economic impact needs to be considered. The use of upcycled and re-used materials throughout the project has allowed the team to drastically reduce the overall cost of materials, making the project more financially viable and encouraging others to make such savings through social media. The process also reduces waste from manufacturers who provide materials in return for recognition on the vessel livery, through social media and acknowledgements. Our investigation into improving sustainability drew several conclusions on improving the sustainability of composite manufacture using wooden moulds and flax fibre. If such changes are adopted in the future, the industry can protect itself from future emissions regulations and facilitating future innovation. Finally, the concepts explored and built-upon in this project have implications for the wider composites industry. Cheaper, more sustainable moulds may serve to reduce emissions and energy consumption for large composite companies while also making complex composite manufacturing techniques more accessible for smaller companies.

Sustainability Conclusions

In conclusion, the innovative use of materials enabled the team to significantly reduce the impact on sustainability of our project in terms of the manufacturing methods used to produce the foil. The reduction in global warming emissions and energy consumption of 94.30% and 83.83% respectively over our baseline shows that we have achieved one of our aims of improving the sustainability of Moth manufacture. Considering that foils for Moth racing are generally bespoke items, the use of wooden moulds could drastically reduce the impact on emissions and energy consumption that the industry has. It is also important to note that this LCA is a conservative estimate due to the assumptions made.

Sustainability analysis directly contributed to the selection of wood as a mould material. The data shown in Figure 33, clearly visualises the drastic improvement in sustainability parameters that this change in material enabled the team to achieve.

6. REFERENCES

[1] H. Zhang, Q. Wu, Y. Liu, B. Huang and G. Wang, "Free vibration analysis of composite foils with different ply angles based on beam theory," *Ocean Engineering,* p. 108854, 2021.

[2] M. Somireddy, C. V. Singh and A. Czekanski, "Analysis of the Material Behaviour of 3D printed Laminates Via FFF," *Experimental Mechanics,* vol. 59, pp. 871-881, 2019.

[3] A. Dutta, M. K. Hagnell and M. Åkermo, "Interply friction between unidirectional carbon/epoxy prepreg plies: Influence of fibre orientation," *Composites Part A: Applied Science and Manufacturing,* vol. 166, p. 107375, 2023.

[4] G. Welch and G. Bishop, "An Introduction to the Kalman Filter," University of North Carolina, 2006.

[5] K. J. Aström and R. M. Murray, Feedback Systems. An Introduction for Scientists and Engineers, Princeton University Press, 2009.

[6] B. J. Belime, "An hydrofoil control system for the SR02 vessel in the scope of the Técnico Solar Boat Project," Tecnico Lisboa, Lisboa, 2020.

[7] R. M. Murray, Optimization-Based Control, California Institute of Technology, 2009.

[8] MathWorks, "Gain Scheduling Basics," MathWorks, 2024. [Online]. Available: https://uk.mathworks.com/help/control/ug/gain-scheduled-control-systems.html. [Accessed 5 2024].

[9] MathWorks, "lqr," MathWorks, 2024. [Online]. Available: https://uk.mathworks.com/help/control/ref/lti.lqr.html. [Accessed 5 2024].

[10] -https://library.wur.nl/WebQuery/titel/2100133 (Accessed: 08/02/2024)

[11]https://www.researchgate.net/publication/363575090_Reducing_Global_Warming_Potential_Impact_of_Bio-Based_Composites_Based_of_LCA (Accessed: 09/02/2024)

[12] - https://www.sciencedirect.com/science/article/pii/S2214993721001202 (Accessed: 12/02/2024)

[13] - https://www.iccm-central.org/Proceedings/ICCM18proceedings/data/2.%20Oral%20Presentation/Aug23%28Tuesday%29/T34%20Processing%20of%20Out-of-autoclave%20Prepregs/T34-2-AF1510.pdf (Accessed: 12/02/2024)

[14]https://www.researchgate.net/publication/342297471_A_Preliminary_Environmental_Assessment_of_Epoxidized_Sucrose_Soyate_ESS-Based_Biocomposite (Accessed: 01/03/2024)

[15] - https://allianceflaxlinenhemp.eu/en/european-flax-environmentally-responsible# (Accessed: 12/02/2024)

[16] - https://www.diva-portal.org/smash/get/diva2:1262794/FULLTEXT01.pdf (Accessed: 12/02/2024)

[17] - https://www.mdpi.com/2227-9717/8/1/48#:~:text=Thus%2C%20bio%2Dresins%20are%20resins,well%20as%20residual%20agricultural%20waste. (Accessed: 01/03/2024)

A. APPENDIX A - MS360 LCA

A.1. Boat life cycle assessment discussion

MS360 LCA tool provides an extensive list of the commonly used materials in the marine industry, including a wide range of bio-based materials. This allowing the process of lifecycle assessment to be more accessible to manufacturers different level of expertise. The results are easy to interpret with the visualisations provided in the results dashboard.

The tool was intuitive to use for foil manufacture and no problems were encountered.

A.2. Boat life cycle assessment scheme

The parts detailed below are the parts assessed in our LCA.

Parameter	Samples	Mold	Foil	Control	Total
Global warming - Fossil, kg CO2e	62.68	40.11	111.97	91.5	306.26
Global warming - Non-Fossil, kg CO2e	0.76	-53.76	-2.63	-	-55.63
Mineral Resource Scarcity, kg Cue	0.13	0.09	0.21	-	0.43
Energy Consumption - Non-renewable, MJ	1553.62	1027.32	2683.59	1600	6872.53
Energy Consumption - Renewable, MJ	261.56	817.79	417.32	-	1496.67
Water Consumption [m^3]	4.08	0.94	6.19	-	15.16
Marine Eutrophication, kg Ne	0.04	0.01	0.07	-	0.15
Waste Production, %	84.86%	57.54%	85.56%	-	66.09%

A.3. Overall results & CO2 equivalent impact

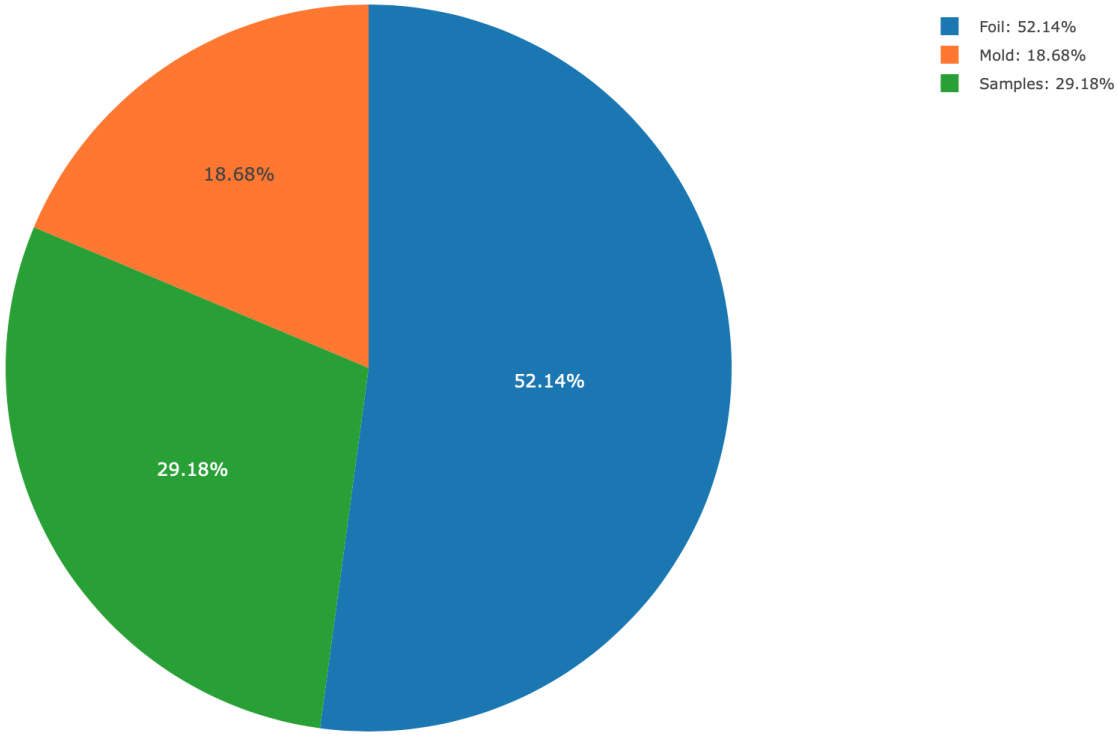

Figure 35 - Global Warming Fossil

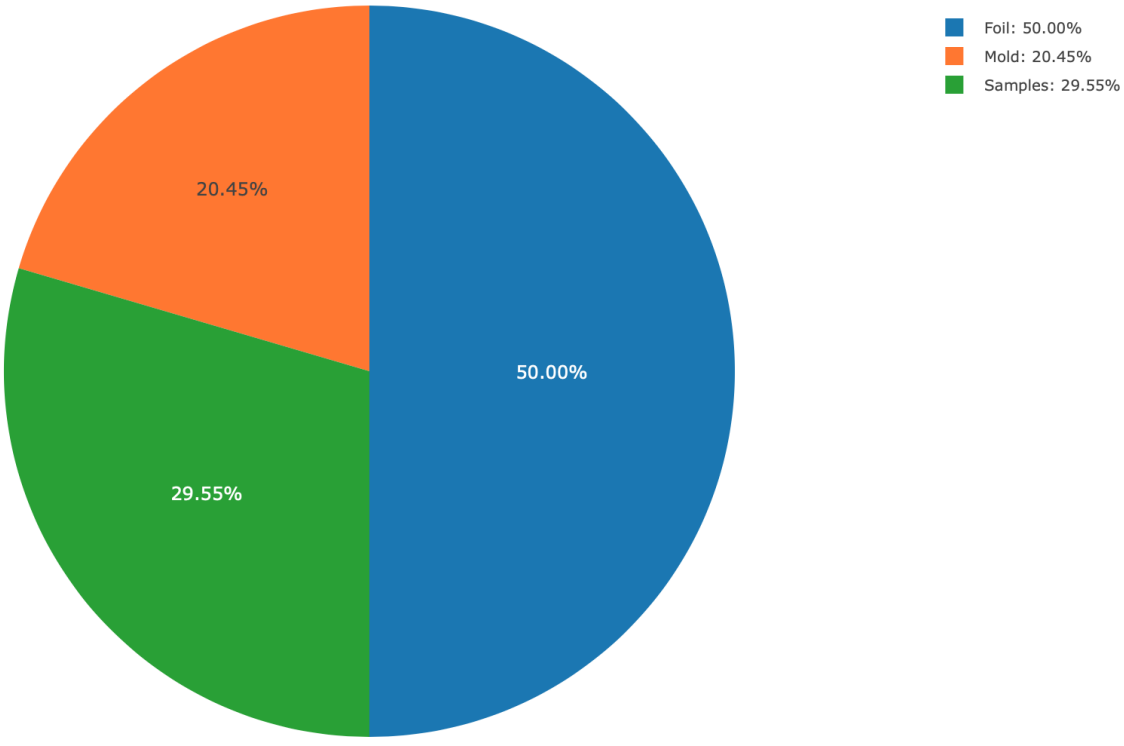

Figure 36 - Mineral Resource Scarcity

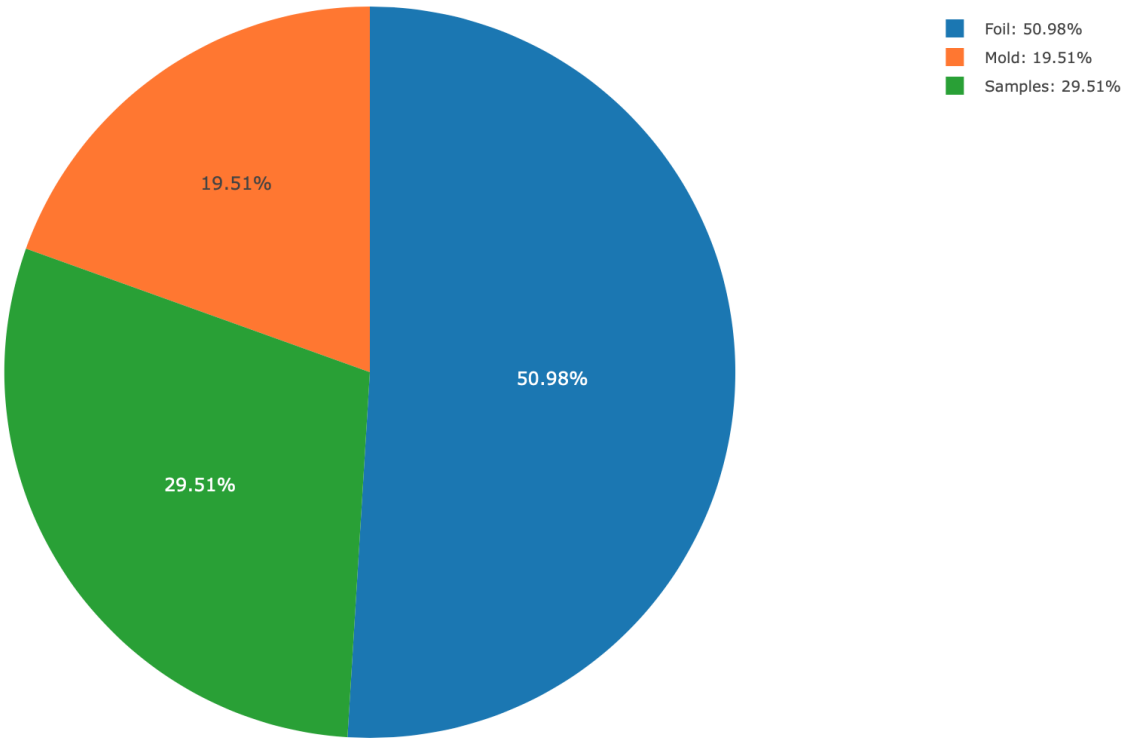

Figure 37 - Energy Consumption – Non-renewable

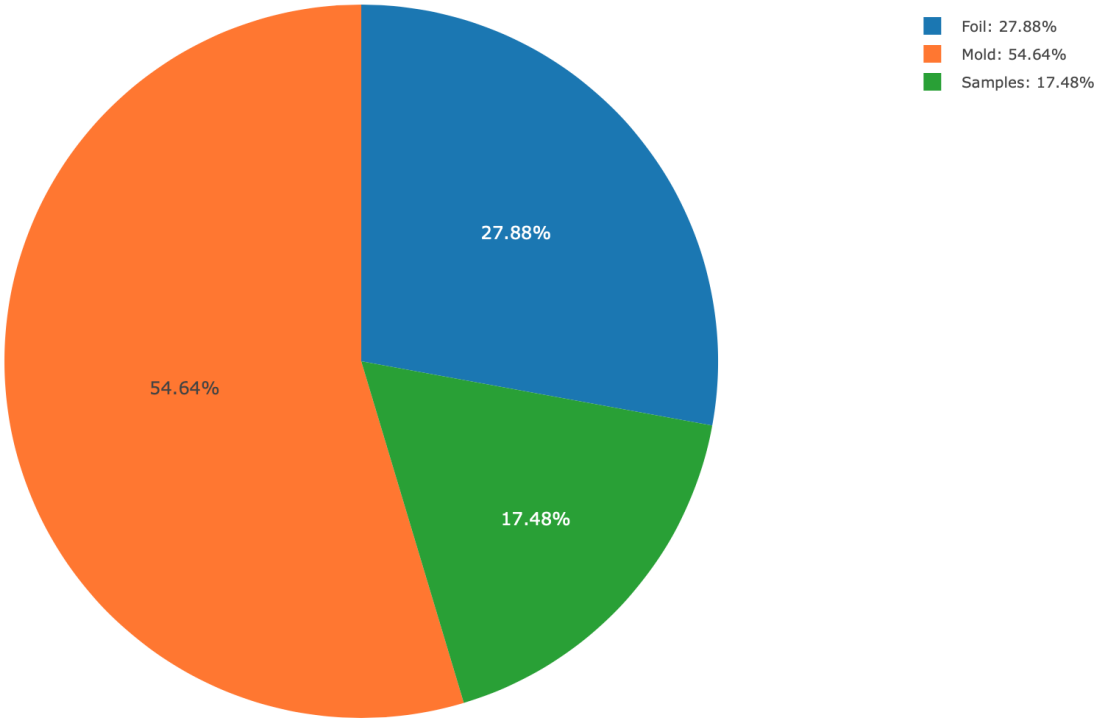

Figure 38 - Energy Consumption – renewable

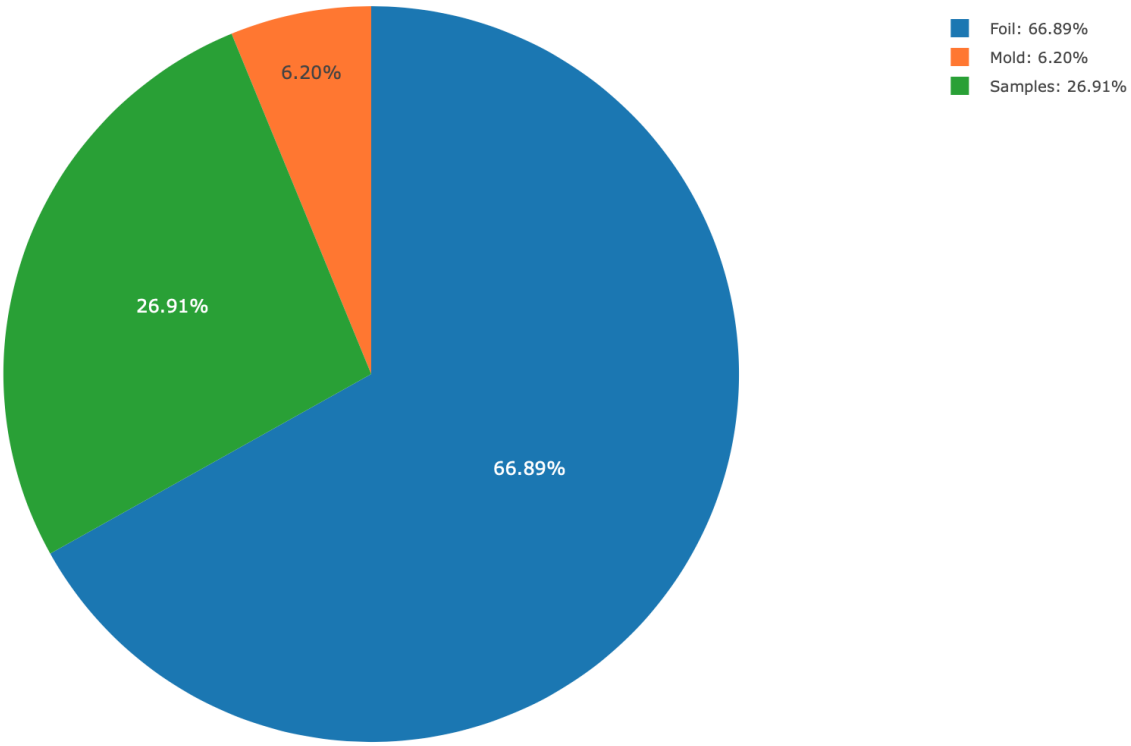

Figure 39 - Water Consumption

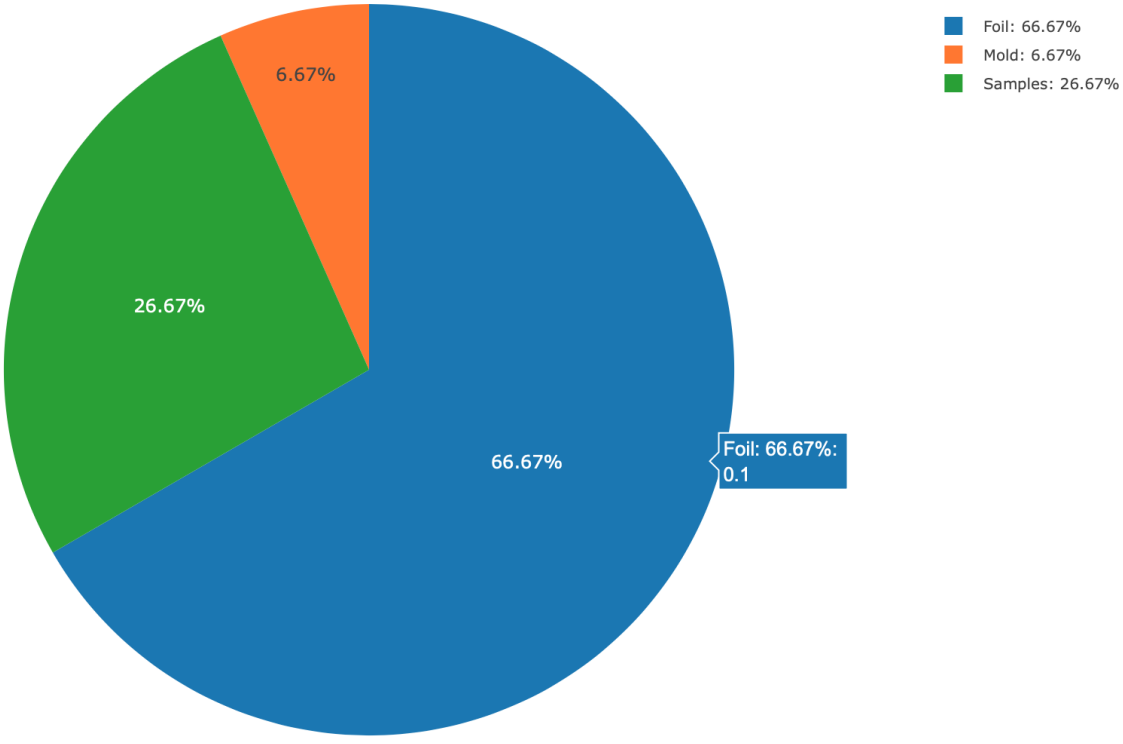

Figure 40 - Marine Eutrophication

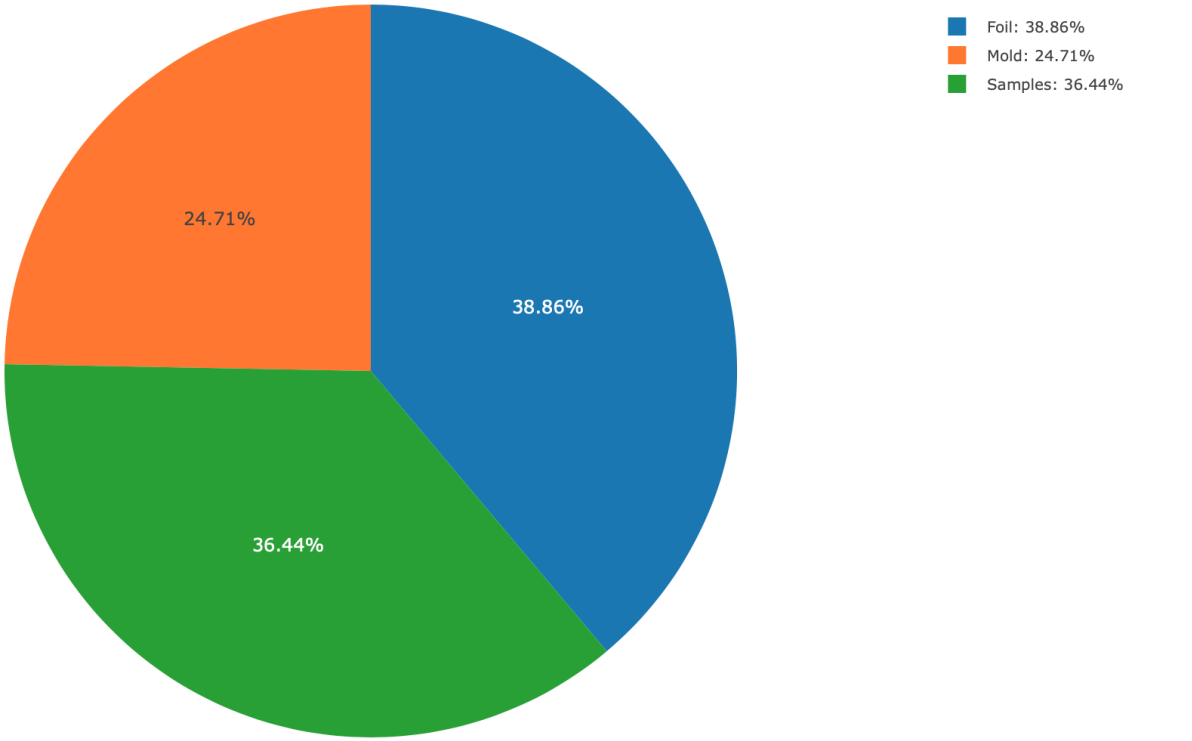

Figure 41 - Waste Production